Astron Astrophys Rev (2015) 23:3
DOI 10.1007/s00159-015-0083-5

REVIEW ARTICLE

Radio emission from supernova remnants

Gloria Dubner[1] · **Elsa Giacani**[1]

Received: 17 March 2015 / Published online: 16 September 2015

Abstract The explosion of a supernova releases almost instantaneously about 10^{51} ergs of mechanic energy, changing irreversibly the physical and chemical properties of large regions in the galaxies. The stellar ejecta, the nebula resulting from the powerful shock waves, and sometimes a compact stellar remnant, constitute a supernova remnant (SNR). They can radiate their energy across the whole electromagnetic spectrum, but the great majority are radio sources. Almost 70 years after the first detection of radio emission coming from an SNR, great progress has been achieved in the comprehension of their physical characteristics and evolution. We review the present knowledge of different aspects of radio remnants, focusing on sources of the Milky Way and the Magellanic Clouds, where the SNRs can be spatially resolved. We present a brief overview of theoretical background, analyze morphology and polarization properties, and review and critically discuss different methods applied to determine the radio spectrum and distances. The consequences of the interaction between the SNR shocks and the surrounding medium are examined, including the question of whether SNRs can trigger the formation of new stars. Cases of multispectral comparison are presented. A section is devoted to reviewing recent results of radio SNRs in the Magellanic Clouds, with particular emphasis on the radio properties of SN 1987A, an ideal laboratory to investigate dynamical evolution of an SNR in near real time. The review concludes

G. Dubner and E. Giacani are members of the "Carrera del Investigador Científico" of CONICET, Argentina.

✉ Gloria Dubner
gdubner@iafe.uba.ar

Elsa Giacani
egiacani@iafe.uba.ar

[1] Instituto de Astronomía y Física del Espacio (IAFE), CONICET-UBA, Casilla de Correo 67, Suc. 28, 1428 Buenos Aires, Argentina

with a summary of issues on radio SNRs that deserve further study, and analysis of the prospects for future research with the latest-generation radio telescopes.

Keywords ISM: supernova remnants · Radio continuum: ISM · Radiation mechanisms: non-thermal · ISM: cosmic rays

1 Introduction

In 1919, the Swedish astronomer Knut Lundmark put forward the hypothesis that "along with ordinary novae, on rare occasions stars flare up that are tens of thousands of times as bright at maximum". Zwicky and Baade proposed in 1934 that such stars be called *supernovae*, and though in the opinion of Shklovsky the name was rather absurd, it was rapidly popularized and now universally designates an event of stellar explosion (Shklovsky 1978).

Supernovae (SNe) can be broadly classified into two big groups depending on the explosion mechanism: the Type Ia are the result of a runaway thermonuclear explosion of a degenerate carbon–oxygen stellar core (most likely a white dwarf in a binary system). The specific progenitor systems and the processes that lead to their ignition have not yet been clearly identified for these SNe as recently reviewed by Maoz et al. (2014). The other big group of SNe involves Types Ib, Ic and II, which are the product of gravitational core collapse of massive stars (initial mass $M \geq 8\,\mathrm{M}_{\odot}$) that have exhausted all their nuclear fuel. If the stellar core contains between 1.4 and 3 $\mathrm{M}_{\odot}$, the compact remnant is a neutron star, while if the mass of the collapsed core is larger than 3 $\mathrm{M}_{\odot}$, a black hole is formed. As summarized in Smartt (2009), there is a diversity of evolutionary scenarios, where metallicity, binarity, and rotation may play important roles in determining the end states, what kind of compact remnant leaves, etc. As a general introduction to the radio SNRs and their connection with the explosion mechanisms that give birth to them, Fig. 1 summarizes the types of SNe, their precursors and possible remnants.

Independently of the type of explosion, about 10^{51} ergs of mechanic energy are suddenly deposited in the interstellar medium and several tens of solar masses of stellar material are ejected. The outer layers of the star blow off in all directions and the enormous explosion power imparts great velocities to the portions of the expelled envelope. A nebula is formed that expands at a speed that can reach 5000 to 10 000 km s^{-1}. This high expansion velocity is the main sign that distinguishes the remnants of supernova outbursts from other nebulosity. Hundreds or thousands of years later, the ejected material will begin to be slow down by the ambient medium, the velocity will start to fall to hundreds or even tens of km s^{-1}, and ultimately will disperse and merge with the surrounding gas. But through thousands of years, a distinctive nebula, the supernova remnant (SNR), persists and can, eventually, be detected across the whole electromagnetic spectrum from radio to gamma rays. The neutron stars, the compact objects left by most of the supernova explosions, will continue radiating energy for many more millions of years.

Before the advent of radio astronomy, only two SNRs were known, the Crab Nebula and Kepler's SNR. Radio observations played a crucial role in the discovery

Explosion	THERMONUCLEAR	CORE-COLLAPSE		
Early Spectra	No Hydrogen Silicon	Hydrogen	No Hydrogen No Silicon Helium rich	No Hydrogen No Silicon Helium poor
SN Type	Ia	II	Ib	Ic
Stellar precursor	White dwarf in binary system	Stars with initial mass: 8 – 17 Mo	8 – 30 Mo	8 – 30 Mo
Compact remnant	None	NS (1.4< M <3 Mo)	NS or BH (M >3 Mo)	NS or BH
Radio Remnant	Shell	Shell and/or PWN	Shell and/or PWN	Shell and/or PWN
Examples	Tycho's, SN1006	Shell-type: Cas A PWN: Crab Shell + PWN: G0.9+0.1		

Fig. 1 Diagram summarizing the types of SN explosion, their precursors and possible radio remnants. NS is the acronym of neutron star, BH of black hole and PWN of pulsar wind nebula. Mass limits are taken from Smartt (2009). Mass quoted for NS and BH correspond to the compact core

and investigation of SNRs and their environs, revolutionizing the knowledge in the field.

In 1948, at the very opening era of radio astronomy, the British astronomers, Sir Martin Ryle and Graham Smith (Ryle and Smith 1948), detected an unusually bright radio source, Cassiopeia A (Cas A). The flux of this source was comparable to the radio flux of the quiet Sun at meter wavelengths, and it seemed to come from a place where no optical emission was apparent. Faint, filamentary optical emission was only later discovered by Baade and Minkowski (Baade and Minkowski 1954) from plates acquired in 1951 with the 200 in. Palomar telescope. But soon after 1948, several radio sources associated with SNRs were found in our Galaxy: the Crab Nebula, the remnants of the Tycho and Kepler supernovae, and a filamentary nebulae in the constellation of Cygnus. Then arose the fundamental question of the nature of those radio waves, since their radiation had nothing in common with thermal black body radiation, but rather was more akin to the non-thermal Galactic radiation detected in the early years of radio astronomy by Karl Jansky and Grote Reber (Jansky 1933; Reber 1944). There was clearly a complete disagreement between the observed radio spectra of SNRs and those of thermal radio sources. The correct idea explaining radio emission of SNRs was proposed in 1950 by Alfvén and Herlofson (Alfvén and Herlofson 1950), and independently by Kiepenheuer (Kiepenheuer 1950). The answer was synchrotron radiation. The synchrotron nature was later confirmed by the detection of polarization in the Crab Nebula by Mayer et al. (1957).

In the following years, radio continuum surveys carried out at different frequencies were the main tool for identifying new SNRs through their non-thermal spectrum, the "fingerprint" in this energy band. Whenever the instruments improve in sensitivity and

angular resolution, new sources are found and this field is in continuous progress. From the very first lists of SNR candidates published by Aizu and Tabara (1967) and Poveda and Woltjer (1968) (with 25 SNRs listed), superseded by Milne (1970) (who increased the list to 94 members in the Milky Way and 3 in the Large Magellanic Cloud), Downes (1971), Ilovaisky and Lequeux (1972), Clark and Caswell (1976), numerous works reported the discovery of new sources and refined their classifications. A step forward came from the contribution of Brogan et al. (2006), who based on high-quality low-frequency radio observations disclosed the presence of 31 new SNRs in the inner Galaxy, increasing by about 15 % of the total number of Galactic SNRs known by then. At the present time, there are 294 firmly classified SNRs in our Galaxy, as compiled and permanently updated by Green (2014).[1] of which the large majority (∼95 %) are radio sources. Also, Ferrand and Safi-Harb (2012) keep an updated census of high-energy observations of Galactic SNRs,[2] listing their physical properties along with a summary of observations of these remnants with various X-ray and γ-ray observatories.

It has to be noted that after years of searching, the total number of detected SNRs in the Milky Way is significantly smaller than expected. A number at least three times greater of SNRs is statistically predicted on the basis of OB star count, pulsar birth rates, SN rates in other local group galaxies, and predicted lifetime of radio synchrotron-emitting sources in the sky. Such deficit is generally attributed to selection effects (Brogan et al. 2006), when old, faint, large remnants, as well as young, small sources, remain below the threshold in sensitivity and/or spatial resolution of the large Galactic surveys performed up to now.

2 A brief overview of the theory needed to understand radio emission from SNRs

Many good text books present the physical background of synchrotron emission in the radio astronomical context (e.g. Pacholczyk 1970; Moffet 1975; Verschuur and Kellermann 1988; Harwit 1988; Rohlfs 1990; Rohlfs and Wilson 1996), and more recently a good synthesis is presented in the review of SNRs at high energies by Reynolds (2008). Here, we summarize just the basic results needed for the interpretation of observational data with a brief guide to infer intrinsic properties and physical conditions of a source from the observed parameters. Readers not interested in the background aspects can jump to Sect. 3.

2.1 Synchrotron radiation

A single relativistic electron moving in an external magnetic field B will emit continuum spectrum radiation. The frequency near which the emission reaches its maximum intensity is called the critical frequency for synchrotron emission and is defined as:

[1] http://www.mrao.cam.ac.uk/surveys/snrs/.

[2] http://www.physics.umanitoba.ca/snr/SNRcat/.

$$\nu_c = \frac{3e}{4\pi mc} B_\perp \left(\frac{E}{mc^2}\right)^2 = C_1 B_\perp E^2, \quad (1)$$

where the constant $C_1 = 6.266 \times 10^{18}$ in cgs units or $C_1 = 16.08$ when ν is in MHz, B in microgauss and E in GeV (Moffet 1975). For example, if we observe radiation at ∼1500 MHz and assume a typical B field of ∼10 μG, we can conclude that such radiation was produced by electrons with an energy of 3 GeV. It can be shown that the time required for an electron to lose half of its energy is $t_{1/2} = C_3/(B^2\ E_0)$, where $C_3 = 8.35 \times 10^9$ years when B is in μG and E is in GeV. Then the electron of our example would radiate half of its energy in about 30 million years. For the Crab Nebula, with B ∼500 μG, the time to lose a substantial portion of its energy for an electron radiating in radio (500 MHz) is ∼100 000 years, for an optical photon (600 nm) about 100 years, and for X-rays (4 keV) ∼2.4 years. Such short lifetimes (much shorter than the age of the Crab Nebula) implies that the pulsar is permanently feeding energy into relativistic electrons.

Actually, relativistic particles are not alone, but in an ensemble. The synchrotron radiation that an observer detects from a particular volume element of a radio source comes from all the electrons with the same pitch angle. We can assume that the source consists of a volume V containing a tangled magnetic field with average strength B, in which there are electrons with an energy density with power law distribution (as the empirical evidence of the cosmic rays close to the Earth shows) $n(E)\mathrm{d}E = n_0 E^{-\gamma}\mathrm{d}E$ between a range of energies $E_1 \leq E \leq E_2$ to avoid divergences in the extremes. In this case, it can be shown that the emitted radiation has a spectrum $\epsilon_\nu \propto \nu^{-\frac{(\gamma-1)}{2}} = \nu^{-\alpha}$, with $\alpha = \frac{(\gamma-1)}{2}$ the emission spectral index . It can be easily concluded that the power law of the SNRs radio spectrum simply reflects the power law energy spectrum of the relativistic particles responsible for the radio waves that we observe. After carrying out the corresponding calculations, it can be shown that the flux density of a synchrotron source with a volume V follows the expression:

$$S(\nu) = 0.017 a(\alpha) V B^{(\alpha+1)} \left(\frac{6.26 \times 10^{18}}{\nu(Hz)}\right)^{\alpha} \mathrm{Jy}, \quad (2)$$

where $a(\alpha)$ takes values like 0.283 for a spectral index $\alpha = 0$; 0.103 for $\alpha = 0.5$; or 0.085 for $\alpha = 0.75$ (Rohlfs 1990). The convention adopted here is that the flux density $\mathrm{S}_\nu \propto \nu^{-\alpha}$ following Rohlfs (1990).

During the evolution of a remnant, the magnetic field strength will decrease producing a secular decay of the flux density for young radio sources (Shklovsky 1960a). The exact rate depends on the field configuration, but assuming that the magnetic flux remains constant, $B(R)$ is proportional to R^{-2} for an adiabatic expanding nebula of radius R. Then, the flux density should decrease with R as $S_\nu \propto R^{-2\gamma}$, which can be expressed as a function of time as $\mathrm{S}_\nu \propto \mathrm{t}^{-4\gamma/5}$. Therefore, it is expected that the flux density decreases with time as:

$$\dot{S}_\nu / S_\nu = -\frac{4\gamma}{5t}. \quad (3)$$

This result is a rough approximation for a young source evolving into a uniform medium. A more rigorous result can be obtained by numerically computing the radio emission along with the hydrodynamic evolution of the SNR. In some cases for very young remnants (less than ∼100 years), the radio emission can follow the opposite behavior and increase the flux with time. This is the case for the example of the youngest SNR observed in our Galaxy, G1.9+0.3, whose flux density increased by a factor of 1.25 over 13 years at 1.4 GHz (Green et al. 2008), and the SN 1987A in the Magellanic Cloud where the flux density increases in an exponential way with an average annual rate (measured in the year 20 since the SN explosion) of the order of 15 % at different radio frequencies (Zanardo et al. 2010).

2.2 Particle acceleration

An important question is what accelerates the particles to relativistic speeds in an SNR. If the remnant contains a pulsar, the answer is clear; it is the pulsar which supplies freshly accelerated electrons over the full lifetime of the SNR. But what happens with SNRs that do not have a neutron star in their interior? If the amount of material picked up by the supernova shock is large compared to the ejecta mass, then the particles can be accelerated in the shock waves.

The basis of all theories to explain acceleration mechanisms in shock waves is that particles can gain energy in collisions with irregularities of the magnetic field. Bell (1978a, b) and Blandford and Ostriker (1978) proposed that the most efficient process is diffusive shock acceleration (DSA), where electrons gain energy after multiple crossing through a shock wave (Fermi 1949). For energetically unimportant test particles which do not influence the flow structure (the so-called test particle limit), the synchrotron spectral index is fixed by the shock compression ratio r by $\alpha = 3/(2(r-1))$. In the case of strong shocks with a compression ratio of 4, this mechanism predicts a spectral index $\alpha = 0.5$ for the radio flux density S. Coincidences and departures from this theoretical prediction are discussed in Sect. 5. For extensive discussions and reviews of standard and nonlinear particle acceleration theories, see for example Blandford and Eichler (1987), Reynolds (2008), Malkov and O'C Drury (2001), Reynolds (2011), Jones (2011), Urošević (2014), and references therein.

2.3 Magnetic field

It was earlier theoretically suggested by Laan (1962) and later reinforced by Whiteoak and Gardner (1968) through a polarization study that the magnetic field responsible for the synchrotron emission observed in SNRs was the interstellar field compressed by the explosion. The hypothesis was plausible because even a relatively weak compression of few micro Gauss of the ambient magnetic field would result in an observable radio source, due to the strong dependence of volume emissivity on the magnetic field strength.

Years later, however, indirect observational arguments, like the thickness of the X-ray rims in the SNRs Cas A, Kepler, Tycho, RCW 86 and SN 1006 (e.g. Jun and Norman 1996; Parizot et al. 2006; Ballet 2006, and references therein), and the rapid

variability (on timescale of few years) observed in X-ray spots in G347.3−0.5 (SNR RXJ1713.7-3946) (Uchiyama et al. 2007) and in Cas A (Patnaude and Fesen 2007), pointed to the fact that the magnetic fields must be from tens to hundreds of times more intense than expected from adiabatic compression of the interstellar magnetic field and some extra mechanism of amplification is required. Such mechanism must have little connection with the past of the SNR, since the seven studied cases have different progenitors, different explosion types (SNe types II and Ia), and contain contain or not a central neutron star, etc., but all of them require considerable magnetic field amplification to explain the observations.

Several mechanisms have been proposed that amplify the magnetic field. Schure et al. (2012) and Reynolds et al. (2012) present reviews on observations and various theories on magnetic field amplification in the presence of a cosmic ray population, showing that cosmic ray streaming can induce instabilities that act to amplify the magnetic field. Some of the proposed models include amplification due to flow instablities (of the Rayleigh–Taylor or Rankine–Hugoniot class) between the mean flow and clouds in the circumstellar and/or interstellar medium (e.g. Jun et al. 1995; Jun and Norman 1996); amplification as a result of very efficient acceleration of nuclear cosmic rays at the outer shock (Völk et al. 2005, and references therein); turbulent amplification driven by cosmic ray pressure (Beresnyak et al. 2009; Drury and Downes 2012); nonlinear DSA (Schure et al. 2012, and references therein), etc. However, the global problem about the origin, properties and evolution of the magnetic field in SNRs is still a matter of debate.

2.4 The energy stored in particles and magnetic fields

For an SNR, it is of interest to determine the energy content. This can be done by integrating over the electron spectrum between the energies E_1 and E_2. If evidence of a cutoff is observed at one end or the other of the radio spectrum, the total electron energy can be expressed in terms of the cutoff frequencies ν_1 and ν_2 (the critical frequencies for the cutoff energies) and α, the spectral index of the source. By assuming that each electron radiates only at its critical frequency, we obtain an expression for the electron energy:

$$U_e = \frac{L\, C_1^{1/2}}{C_3 B^{3/2}} \frac{(2-2\alpha)}{(1-2\alpha)} \frac{\nu_2^{1/2-\alpha} - \nu_1^{1/2-\alpha}}{\nu_2^{1-\alpha} - \nu_1^{1-\alpha}} \quad (\text{if } \alpha \neq 0.5 \text{ or } 1), \tag{4}$$

where L is the total luminosity of the source derived from the observed flux density S ($L = 4\pi d^2 S$ assuming isotropic radiation and that the distance d to the source is known), the constant C_1 is as defined above, $C_3 = 2.368 \times 10^{-3}$ in cgs units and B is the average strength of the magnetic field. The magnetic field may not be measured directly, but its value may sometimes be inferred (at least to an order of magnitude, as shown below). Observations at different frequencies provide an estimate of the spectral index α.

The lower cutoff energy can be taken equal to the electron rest mass energy (an electron that is not relativistic will not produce synchrotron radiation). Observations

show departures from a power law spectrum in the range from tens to few hundreds of MHz. Therefore, a lower cutoff frequency of 10^7 Hz is often assumed. For the upper cutoff, if the source under study has X-ray measurements, the break frequency derived from the intersection of radio and X-ray spectral slopes can be used as upper frequency for radio emission. If there is no other indication, it is customary to use $\sim 10^{10}$ or 10^{11} Hz as the upper cutoff.

The energy of a source that emits synchrotron radiation can be mainly contained in two forms, as kinetic energy of the relativistic particles $U_{\rm part}$ and as energy stored in the magnetic field $U_{\rm mag}$ (thermal radio radiation is negligible, therefore thermal energy will be small compared to the former, and gravitational energy is probably the source of particles and magnetic energies, but almost nothing is known about it and is not considered).

To estimate the energy stored in particles, we have to take into account that in addition to electrons, there must be protons and other energetic baryons in the radiating source (though heavy particles emit negligible amounts of radiation because they are accelerated much less by the Lorentz force). Therefore, $U_{\rm part} = \eta U_e$, where η is a factor that takes all other particles into account. From various methods, η has been estimated to be 50 (the value from cosmic rays near Earth) or 100 (from models applied to radio sources in our Galaxy, e.g. Burbidge 1959). Fortunately, as shown below, this uncertainty does not have a strong effect on the fundamental conclusions.

On the other hand, the energy stored in the magnetic field for a source of volume V is: $U_{\rm mag} = V B^2/8\pi$. Therefore,

$$U_{\rm tot} = U_{\rm part} + U_{\rm mag} = \eta A L B^{-3/2} + V B^2/8\pi, \tag{5}$$

where A takes into account the constants C_1, C_3 and the shape factor in frequency.

It can be noticed that the energy stored in particles, proportional to $B^{-3/2}$, will dominate for small field strengths, while the magnetic energy ($\propto B^2$) dominates for large fields. In consequence, the total energy $U_{\rm tot}$ has a minimum for a magnetic field intensity

$$B(U_{\rm min}) = \left(\frac{6\pi a A L}{V}\right)^{2/7}, \tag{6}$$

for which $U_{\rm part}/U_{\rm mag} = 4/3$. Thus, the minimum total energy to produce the observed radio emission corresponds quite closely to an equipartition between relativistic particles and magnetic fields. If the magnetic field is exactly that of equipartition, then $U_{\rm min} = 0.5(\eta A L)^{4/7} V^{3/7}$. In this way, we can obtain a firm lower limit of the energy requirements of a synchrotron source. Examples of the use of these relations can be found in Frail et al. (1996a) for the PWN in W44, Dubner et al. (2000) for SNR W28, or in Castelletti et al. (2007) for W44.

The relations presented above are useful to get first estimates of energy content and magnetic field strength in radio SNRs, but it should be made clear that there is no physical justification for the energy components of the source being close to equipartition. It has been conjectured that motions in the plasma may stretch and tangle the magnetic fields and turbulent motions might also accelerate particles to high

energies, thus taking the plasma closer to equipartition, but these are only conjectures and, in fact, these radio sources might be far from equipartition.

2.5 Dynamical evolution

Since the separation of the SNR evolution in four distinct phases originally proposed by Woltjer (1972), the scheme was maintained up to the present and is generally defined as follows:

- *Free expansion phase* This phase occurs when the shock wave created by the explosion moves outwards into the interstellar medium (ISM) at highly supersonic speed and compressed interstellar gas accumulates behind the strong shock. This material is separated from the ejected stellar material by the contact discontinuity (a surface between two different materials with similar pressure and velocity, but different density). Behind the contact discontinuity, a reverse shock starts to form in the ejected stellar material. After some time, the accumulated mass of the ISM compressed between the forward shock and the contact discontinuity equals the ejected mass of stellar material, and it starts affecting the expansion of the SNR, marking the beginning of:
- *The adiabatic expansion or Sedov–Taylor phase* Here, the expansion is driven by the thermal pressure of the hot gas. In this stage, after the passage of the reverse shock, the interior of the SNR is so hot that the energy losses by radiation are very small. Since all atoms are ionized, there is no recombination, and the cooling of the gas is only due to the expansion. This stage has an exact self-similar solution (Taylor 1950; Sedov 1959). Later, as the SNR expands and cools adiabatically, it reaches a critical temperature of about 10^6 K, the ionized atoms start capturing free electrons and they can lose their excitation energy by radiation. The radiative losses of energy become significant, setting the end of the adiabatic expansion of the SNR. The efficient radiative cooling decreases the thermal pressure in the post-shock region and the expansion slows down. The SNR enters in the so-called:
- *Snow plough or radiative phase* when more and more interstellar gas is accumulated until the swept-up mass is much larger than the ejected stellar material. Finally, the shell breaks up into individual pieces, probably due to a Rayleigh–Taylor instability (hot thin gas pushes cool dense gas) and the SNR goes into the final phase.
- *Dispersion*, as the expansion velocity decreases to values typical of the interstellar gas and the SNR disperses into the ISM.

This scheme is an oversimplification and, as pointed out by Jones et al. (1998), distinct phases may be brief, may not occur at all, or may occur simultaneously in different regions of the same remnant. A detailed description of the hydrodynamical evolution of SNRs can be found in Lequeux (2005).

Chevalier (1974) developed a set of numerical models to describe the spherically symmetric expansion of an SNR in a uniform medium, providing semi-analytical expressions to estimate expanding radius, age, shock velocity, etc., for different initial and ambient conditions. Although this work was later complemented with many

different variations to consider inhomogeneous surroundings, interaction with circumstellar matter, etc. (e.g. Chevalier 1982b; Truelove and McKee 1999), it is still a classic that can be used as a first approach to derive the physical parameters from observed properties in SNRs. For example, for an initial energy of $E_0 = 3 \times 10^{50}$ ergs, ambient density $n_0 = 1$ cm^{-3} and $B_0 = 3 \times 10^{-6}$ Gauss, the radius and shock velocity of an SNR at late times of evolution (after about 5×10^4 years) can be estimated within the model approximations using the following relations: $R_0 = 21.9\ t_5^{-0.31}$ pc and $v_{sh} = 66.5\ t_5^{-0.69}$ km s^{-1}. Vink (2012) presents a good overview of different analytical models developed for SNRs expanding in various environments.

3 Radio morphology

As already mentioned, the vast majority of SNRs in our Galaxy were first recognized from radio observations. In fact, out of 294 known remnants in our Galaxy, only 20 have not been either detected in the radio band or are poorly defined by current radio observations (Green 2014). The morphology and brightness distribution in SNRs contain important information about the nature of the SNR and its possible hydrodynamical evolution.

Supernova remnants have been traditionally classified based on their radio morphology into three broad categories (see Weiler and Sramek 1988 for a historical perspective on SNR naming conventions). They are:

(a) *Shell-type SNRs*, whose appearance is characterized by a limb-brightened shell or ring formed initially by the ejecta from the SN, and at later times also by swept up surrounding material. The diameter of the shell corresponds to the expanding shock wave produced by the explosion. In this case, the particles responsible for the observed synchrotron radiation are believed to be accelerated at the shock front.

(b) *Filled-center or plerions*, in which the radio brightness is centrally concentrated and is often linearly polarized. In this case, the accelerated particles and magnetic fields responsible for the synchrotron emission are injected by a pulsar created in the supernova event. This pulsar transfers the bulk of its rotational energy in a wind of relativistic particles and Poynting flux that interacts with the surrounding medium creating a synchrotron-emitting nebula named "Pulsar Wind Nebula" (PWN). PWNe can emit non-thermal radiation over the whole electromagnetic spectrum. The Crab Nebula is a prime example of this class of remnants. Figure 2 shows a high-quality, sub-arcsec resolution radio image of the Crab Nebula at 3 GHz, obtained with the Karl Jansky Very Large Array (JVLA, NRAO) as part of a project of simultaneous multi-wavelengths investigation of this source (Krassilchtchikov et al. 2014, Dubner et al. 2015, in preparation. See also Bietenholz et al. 2015). It has to be noted that there are several plerionic SNRs, for which no pulsar has yet been found. For these cases, the detection of the nebula is a strong indication that the powering source must be an undetected pulsar. Gaensler and Slane (2006) presented a complete review of PWNe as seen across the whole electromagnetic spectrum.

(c) *Composite*, for which the SNR appears to have both a shell and an internal non-thermal pulsar driven nebula. As noted by Green (2014), the term "com-

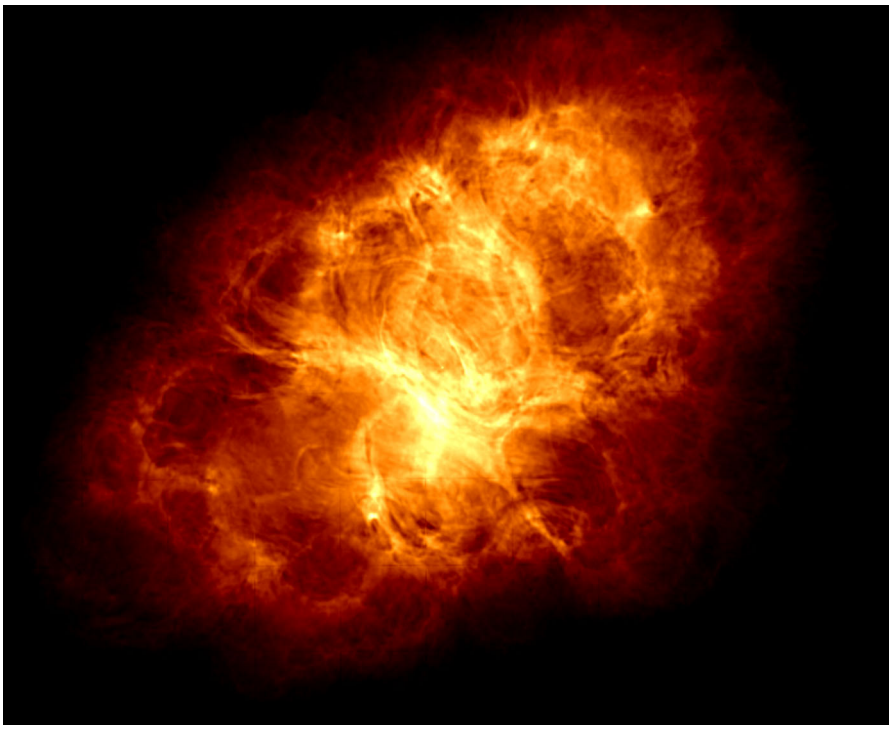

Fig. 2 Detailed radio image of the Crab Nebula, obtained at 3 GHz with the Karl Jansky Very Large Array (NRAO) in the A-configuration. The image has an HPBW of $0''.9 \times 0''.8$ and the rms noise is better than 30 μJy (Dubner et al. 2015 in preparation)

posite" has been also used by some authors to describe SNRs with radio shell and centrally brightened thermal X-ray emission. Such SNRs are also known as "mixed-morphology" (M-M) SNRs (Rho and Petre 1998). Since the physical nature of the X-ray central component of these remnants is completely different from the non-thermal PWNe, we prefer to include them in a fourth morphological class.

(d) *Mixed morphology (M-M)*, SNRs with synchrotron radio shell and central thermal X-ray emission. They have attracted more attention in the last years since several of them appear related to molecular clouds and to γ-ray sources, mostly of hadronic nature (when relativistic particles collide with dense ambient gas producing neutral pions, which decay into γ ray). The catalog by Ferrand and Safi-Harb (2012) lists references for such associations. Vink (2012) summarized their properties. Since new members have been reported in the last couple of years, to keep an updated census of these remnants we list in Table 1 the M-M SNRs in the Milky Way, together with their associations with molecular emission and γ-ray detections.

In the recent compilation of Galactic SNRs by Green (2014), 79 % of remnants are classified as shell type (including the mixed morphology), 12 % as composite, and 5 % as plerions. The rest of the remnants do not fit into any of the aforementioned conventional types, defying the simple spherically symmetric expansion solution.

Table 1 Mixed-morphology SNRs

SNR	Name	Molecular material	OH (1720 MHz) masers	GeV	TeV	Refs.
G0.0+0.0	Sgr A East		Y			1
G6.4−0.1	W28	Y	Y	Y	Y	2–5
G31.9+0.0	3C391	Y	Y	Y		3, 6, 7
G33.6+0.1	Kes 79	Y		Y		8, 9
G34.7−0.4	W44	Y	Y	Y		10–12
G41.1−0.3	3C397	Y				13
G43.3−0.2	W49B	Y		Y	Y	14–16
G49.2−0.7	W51C	Y	Y	Y	Y	17–20
G53.6−2.2	3C400.2					
G65.3+5.7						
G82.2+5.0	W63					
G89.0+4.7	HB 21	Y		Y		21, 22
G93.7−0.2	CTB 104A					
G116.9+0.2	CTB 1					
G132.7+1.3	HB 3	Y				23
G156.2+5.7						
G160.9+2.6	HB 9					
G166.0+4.3	VRO 42.05.01	Y		Y		24, 25
G189.1+3.0	IC443	Y	Y	Y	Y	11, 26–28
G272.2−3.2						
G290.1−0.8	MSH 11-61A					
G304.6+0.1	Kes 17	Y		Y		29–31
G327.4+0.4	Kes27					
G337.8−0.1	Kes 41	Y	Y			32, 33
G344.7−0.1		Y		Y	Y	34–36
G352.7−0.1						37
G357.1−0.1	Tornado	Y	Y	Y		38, 39
G359.1−0.5		Y	Y			40, 41

References: (1) Yusef-Zadeh et al. (1996), (2) Reach et al. (2005), (3) Frail et al. (1996b), (4) Aharonian et al. (2008), (5) Hanabata et al. (2014), (6) Reach and Rho (1999), (7) Castro and Slane (2010), (8) Giacani et al. (2009), (9) Auchettl et al. (2014), (10) Seta et al. (1998), (11) Claussen et al. (1997), (12) Abdo et al. (2010a), (13) Jiang et al. (2010), (14) Zhu et al. (2014), (15) Brun et al. (2011), (16) Abdo et al. (2010b), (17) Koo and Moon (1997), (18) Green et al. (1997), (19) Abdo et al. (2009), (20) Feinstein et al. (2009), (21) Koo et al. (2001), (22) Reichardt et al. (2012), (23) Routledge et al. (1991), (24) Huang and Thaddeus (1986), (25) Araya (2013), (26) Su et al. (2014), (27) Ackermann et al. (2013), (28)Acciari et al. (2009), (29) Combi et al. (2010), (30) Gelfand et al. (2013), (31) Wu et al. (2011), (32) Combi et al. (2008), (33) Koralesky et al. (1998), (34) Giacani et al. (2011), (35) Abdo et al. (2013), (36) Aharonian et al. (2006), (37) Giacani et al. (2009), (38) Lazendic et al. (2004), (39) Castro et al. (2013), (40) Hewitt et al. (2008), (41) Uchida et al. (1992)

With regard to shell-type SNRs, multi-frequency observations of SNRs carried out in the last years with increasing resolution and sensitivity have demonstrated that the actual morphologies of these objects are highly complex and less than 20 % of

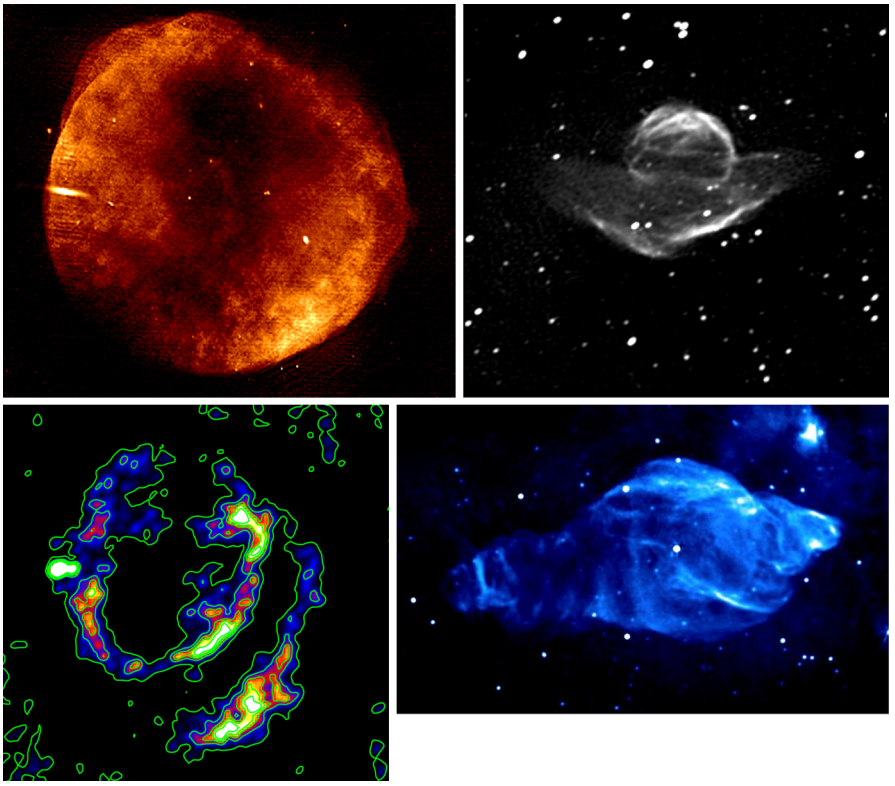

Fig. 3 Radio images of SNRs with a variety of morphologies. *Upper left* SN1006 at 1.4 GHz as taken from Petruk et al. (2009); *upper right* VRO 42.05.01 at 1.4 GHz as extracted from the CGPS public database; *bottom left* G352.7−0.1 at 5 GHz from Giacani et al. (2009); *bottom right* W50 at 1.4 GHz taken from Dubner et al. (1998)

the shell types have an almost complete circular ring appearance. In effect, in radio waves, SNRs exhibit an ample variety of shapes, such as *blow-out:* in which, part of the shell appears to have expanded more rapidly than the rest. An example of this type is the SNR VRO 42.05.01 (G166.0+4.3) (Fig. 3 upper right) that at first sight appears to be two different sources adjoining in the plane of the sky (Landecker et al. 1982), but HI observations demonstrated that it is a single SNR breaking out from a warm medium into a tenuous interstellar cavity (Pineault et al. 1987; Landecker et al. 1989); *barrel-shaped or bilateral:* SNRs characterized by a clear axis of symmetry, low level of emission along this axis, and two bright limbs on either sides (Gaensler 1998). Typical examples of this type are G296.5+10.0 (Giacani et al. 2000) and SN1006 (Reynolds and Gilmore 1986; Petruk et al. 2009) (Fig. 3 upper-left); *multi-shells:* remnants with two or more overlapping rings of emission. Examples of this type are G357.7−0.1 (Manchester 1987), 3C400.2 (Dubner et al. 1994), and G352.1−0.1 (Giacani et al. 2009) (Fig. 3 bottom left).

Another interesting morphology is created when a central compact object injects into an SNR a flow of particles along collimated *bi-polar jets*. This appears to be

the origin of the distorted elongated shape observed in some SNRs, as in SNR W50 (Dubner et al. 1998, Fig. 3 bottom right), in Puppis A (Fig. 9 in Castelletti et al. 2006), and in Cas A (Hwang et al. 2004). In the case of the W50/SS433 system, the radio observations confirmed the connection between the sub-arcsec relativistic jets from SS433 and the extended helical nebula over five orders of magnitude in scale (Dubner et al. 1998). A similar origin was proposed for the "ears" observed in the SNR Puppis A, where the central neutron star would be responsible for the production of collimated outflows that impact on the shell. In the case of Cas A, the marked bi-polar asymmetry, in this case revealed in X-rays, was explained by Hwang et al. (2004) as the result of opposite symmetrical jets produced deep within the progenitor of the SN explosion. The nature of this morphology is the subject of observational and theoretical efforts to explain it.

In the investigation of SNR morphologies, an additional complication is that the observed shape is a two-dimensional projection of a three-dimensional object and depends on their orientation with respect to the line of sight and projection effects. As a curiosity useful to illustrate this point, we refer to the animation of a 3-D vision of the optical emission of the Veil Nebula SNR presented by J. P. Metsavainio.[3] An example of the complications inherent to projection effects when studying the origin of the radio morphology is the case of the Galactic SNR G352.7−0.1 (Fig. 3 bottom left) whose radio emission projected in the sky plane looks like two concentric rings. This shape has been alternately proposed to originate in a "barrel-shaped" type of SNR (Giacani et al. 2009) or from a blow-out scenario, where the SN explosion took place near the border of a molecular cloud (Toledo-Roy et al. 2014).

3.1 Can the SN type be constrained on the basis of the radio morphology of the SNR?

This has been a challenging question for decades. The great diversity of shapes observed in radio SNRs reflects not only different properties of the progenitor star and of the explosion mechanisms, but also echoes the properties of the ambient magnetic field and the matter distribution in the circumstellar and interstellar medium. Disentangling the different causes is a complex task that remains a central question.

Several attempts have been made to infer the type of supernovae on the basis of the observed remnants. In the X-ray domain, Lopez et al. (2009, 2011) developed an observational method to characterize the type of explosion of young SNRs by measuring global and local morphological properties of the X-ray line and thermal emission in numerous young SNRs in our Galaxy and in the Large Magellanic Cloud, finding that the remnants of Type Ia SNe have statistically more spherical and mirror-symmetric thermal X-ray emission than SNRs coming from core-collapse origin. These studies were later extended to infrared (IR) morphology by Peters et al. (2013) through the investigation of the symmetry of the warm dust emission, concluding again that Type Ia SNRs are statistically more circular and mirror symmetric than core-collapse SNRs. This is explained as due to different circumstellar environments and explo-

[3] http://astroanarchy.blogspot.com.

sion geometries of the progenitors. Additional ways of identifying the type of SN have been proposed using the X-ray emission, distinguishing Ia remnants from core-collapse ones by virtue of their ejecta composition (Hughes et al. 1995) (Fe-rich and O-poor SNRs are likely Ia, while SNRs dominated by O and Ne lines with weak Fe L emission are likely core-collapse ones). More recently, Yamaguchi et al. (2014) presented an observational diagnostic to discriminate between progenitor types based on the Fe K-shell X-ray emission. The authors found that in remnants from SN Ia, the Fe-rich ejecta is significantly less ionized than in remnants from core-collapse SNe. Their results also indicate that there is a strong connection between the explosion type and the ambient medium density.

The morphological criteria that seems to work for X-rays and IR to infer the SN type from the SNRs characteristics are clearly useless for radio SNRs. If we blindly apply the "circularity" criterion to Cas A and Tycho's SNR, two circularly symmetric young radio remnants, both of them would be classified as SN Ia, but Cas A is core-collapse and Tycho's is SN Ia. On the other hand, the SNRs SN 1006 and G296.5+10.0 are two perfect examples of "mirror-symmetric" sources, but SN1006 is an SN Ia, while G296.5+10.0 has a central compact object suggesting a core-collapse origin (Gaensler 1998; Harvey-Smith et al. 2010).

One important reason that complicates the connection of a radio SNR with its precursor is that while X-rays may retain information about the characteristics of the exploded star, the complexity of the interaction between the shock front and the ejecta, circumstellar and interstellar matter, can soon mask this information in the radio emission. Once the shock front sweeps up a certain amount of ambient gas, the radio synchrotron emission ignores the explosion properties and it is mostly conditioned by inhomogeneities in the surrounding medium, hydrodynamic instabilities in the flow, turbulence behind the shock, effects of magnetic fields, etc. (e.g. Chevalier 1982a, b; Dwarkadas 2005). Sometimes, the traces left by mass loss episodes of the stellar progenitor can help to identify the class of supernova. The presence of a neutron star inside the remnant and/or the existence of the pulsar wind nebulae is an unquestionable evidence of a core-collapse event. The absence of it, however, does not prove anything because pulsars have high kick velocity (e.g. Hansen and Phinney 1997) and can be outside the SNR far from the explosion site, also central compact objects can be radio silent, etc. An indirect indicator of core-collapse SN is finding the SNR very close to or inmersed in a molecular cloud that might be the birthplace of a massive star that ended its life as SN Ib,c or II.

In summary, the radio morphology alone does not provide a useful tool to distinguish between different types of SNe.

4 Polarization

Radio polarization observations of SNRs provide essential information on the degree of order and orientation of the ordered component of the magnetic field, which themselves influence the morphology of the remnants and the intensity of radiation.

As the radio emission in SNRs is primarily synchrotron, the radiation is linearly polarized; therefore from the observed polarization electric vector, the direction of

the orthogonally aligned magnetic field can in principle be determined. However, in practice, the observed polarization can be highly compromised by Faraday rotation, since the electric field vector of the radiation is rotated during the propagation inside the SNR and the interstellar medium. In the simplest case, the angle of rotation ψ varies proportionally to the square of the wavelength λ, such that $\psi = \mathrm{RM}\ \lambda^2$, with the constant of proportionality, or the rotation measure RM, defined as

$$\mathrm{RM}(\mathrm{rad\ m^{-2}}) = 0.81 \int N(\mathrm{cm^{-3}}) B_{\parallel}(\mu\mathrm{G}) dl(\mathrm{pc}), \tag{7}$$

where N is the thermal electron density and $B_{\parallel}$ the magnetic field component along the line of sight l, and the integral extends along the entire line of sight. The sign of RM is determined by whether $B_{\parallel}$ points toward or away from the observer. In general, observations at three or more wavelengths are necessary to measure the RM without ambiguity and to determine the true position angles of the magnetic field lines.

From the synchrotron theory, the intrinsic degree of linear polarization of the radiation emitted from electrons in a uniform magnetic field is independent of the frequency and given by $P = (2\alpha + 2)/(2\alpha + 10/3)$, where α is the radio spectral index of the radiation (Ginzburg and Syrovatskii 1965; Pacholczyk 1970). For a non-thermal radio source with a spectral index $\alpha = 0.5$, the fractional polarization can reach a maximum theoretical value of about 70 %, but in practice a much lower polarization percentage is usually observed.

The reduction of the observed degree of polarization arises from different physical and instrumental effects, namely beam depolarization as a result of variations of the rotation measure on spatial scales smaller than the antenna beam; bandwidth depolarization, when the polarization angle changes across the receiver bandpass and the resulting non-parallel vectors are averaged; and depths depolarization (also known as differential Faraday rotation) when there is superposition of emission from different depths along the line of sight, either internal or external to the radiating source, which suffers different Faraday rotation. Under these conditions, the dependence of ψ with λ^2 is no longer valid. To mitigate this effect, several models have been proposed by, e.g. Burn (1966) and Sazonov (1973). For a discussion of the basic depolarization mechanism and instrumental effects, see also Gardner and Whiteoak (1966), Milne and Dickel (1975), Milne (1980), and Reich (2006).

Recently, a new tool, called RM Synthesis or spectropolarimetry, has been implemented to recover the polarization structure at multiple Faraday depths along a particular line of sight with the additional advantage that minimizes $n\pi$ ambiguities and bandwidth depolarization (for a more detailed explanation, see Brentjens and Bruyn 2005; Heald et al. 2009). Its application has become viable thanks to technical and computational advances. Most applications of this technique have been for interstellar or extragalactic studies (a good review can be found in Beck 2012) and its utilization for studying magnetic fields in SNRs is a very new field of research. Harvey-Smith et al. (2010) applied this tool to the SNR G296.5+10.0 using data taken with the Australia Telescope Compact Array at frequencies near 1.4 GHz. The Faraday rotation maps (Figure 1 in Harvey-Smith et al. 2010) shows a highly ordered rotation measure structure with an anti-symmetric RM morphology across the remnant. The

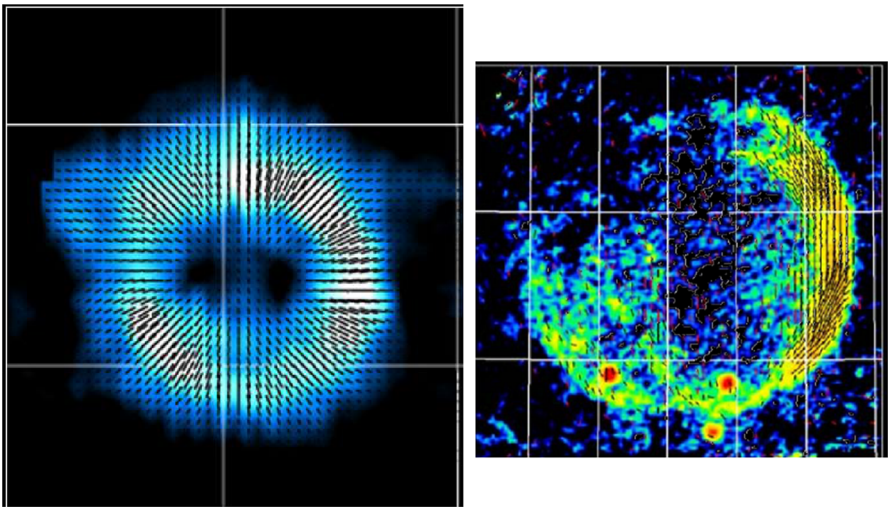

Fig. 4 Radio polarization bars in B-field direction as obtained with the Effelsberg 100-m telescope. *Left* SNR Cas A at 32 GHz; *right* SNR CTB1 at 10.55 GHz (courtesy of W. Reich)

authors proposed that the observed RM pattern is the imprint of an azimuthal magnetic field in the stellar wind of the progenitor star. The expansion of the remnant into such a wind can account for the bilateral morphology of G296.5+10.0 as observed in the radio and X-ray bands.

Even if the radio observations of SNRs are carried out at optimum conditions to minimize the effects mentioned above, the observed degree of polarization in SNRs is still considerably lower than the maximum possible theoretical value. This is an indication that the magnetic fields are primarily disordered. In general, the polarization degree has been found to be between 10 and 15 % (see references in Reynolds and Gilmore 1993), with higher values between 35 and 60 % in some few exceptional cases, as for example in some regions in the Vela SNR (Milne 1980), DA 530 (Landecker et al. 1999), G107.5−1.5 (Kothes 2003), and SN1006 (Reynoso et al. 2013).

At large spatial scale, it has been proposed that the intrinsic orientation of the magnetic field in SNRs, as inferred from the radio observations, shows a typical pattern depending on their age. The earliest observations of the young SNR Cas A showed a convincingly radial magnetic field with respect to the shock front (Mayer and Hollinger 1968), while in the case of the old Vela SNR, the radio polarization map showed a near tangential direction in the brighter emission (Milne 1968). Later on, polarization measurements carried out by Milne (1987) over 27 SNRs confirmed that in young remnants the alignment of the magnetic field is predominantly in the radial direction, whereas the dominant orientation of the field in older remnants is parallel to the shock front or tangled. Subsequent observations have supported this picture (Landecker et al. 1999; Fürst and Reich 2004; Wood et al. 2008). In Fig. 4, we show the intrinsic magnetic field distribution in the SNR Cas A (left) and in CTB1 (right), illustrating two extreme cases of magnetic field distribution, predominantly radial and tangential, respectively.

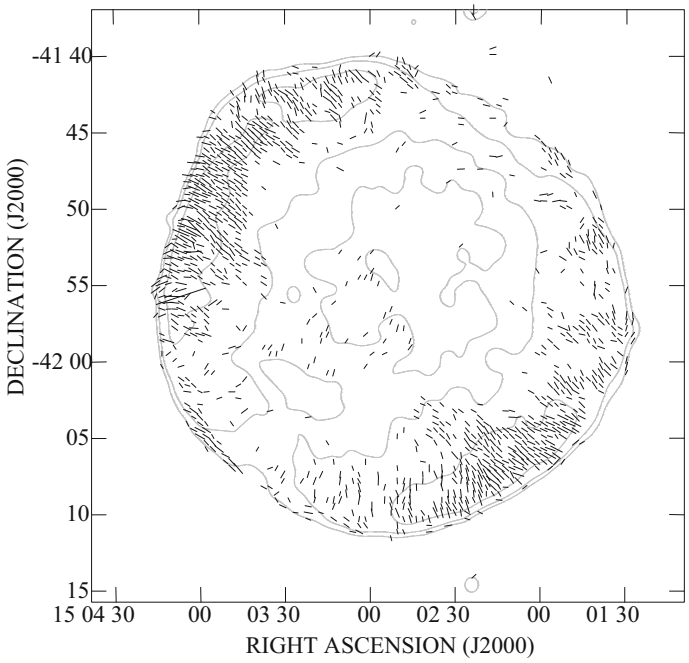

Fig. 5 Magnetic field distribution on SN 1006 at 1.4 GHz (from Reynoso et al. 2013)

The general consensus on the tangentially ordered fields observed in older remnants is that they originate by compression in radiative shocks with large shock compression ratios. Regarding the radial component, however, the origin is still controversial. It has been generally attributed to stretching of Rayleigh–Taylor (R–T) instability fingers that occurs at the contact discontinuity which separates the ejecta from the shocked, more tenuous, circumstellar medium (CSM) (e.g. Jun and Norman 1996). However, polarization observations of SN1006 (Reynoso et al. 2013) show radial orientation near the forward shock (Fig. 5) . This radio polarization study was carried out using data obtained with the VLA and ATCA instruments at 1.4 GHz with an angular resolution of about 10″. The high quality of these data highlights the complex structure of the magnetic field distribution. A notable characteristic in SN1006 is that even when the orientation of the magnetic field vectors across the SNR shell appears to be radial, a large fraction of the magnetic vectors lie parallel to the Galactic plane (whose orientation is perpendicular to the symmetry axis of the bright lobes). Reynoso et al. (2013) conclude from this evidence that the ambient magnetic field must be roughly parallel to the Galactic plane, and the SNR retains some knowledge of the orientation even after the passage of the shock front. Besides, while the degree of polarization in the two bright radio lobes of SN1006 is about 17 %, a value as high as about 60 % is found towards the faint SE border of the remnant. In brief, the brightest radio, X-ray, and TeV features, the NE and SW lobes of SN1006, have the lowest polarization fractions (indicating the presence of a disordered, turbulent magnetic field), while in the SE where the synchrotron emission is faint, the polarization is high (ordered field).

In this case, the authors conclude that the most efficient particle acceleration occurs for shocks in which the magnetic field direction and shock normal are quasi-parallel, while inefficient acceleration and little to no generation of magnetic turbulence are obtained for the quasi-perpendicular case, a result with implications for DSA theories.

Over the past several years, a number of survey projects were launched to map the polarized emission from the Galaxy in great detail. Single-dish as well as synthesis telescopes located in the northern and southern hemispheres are being used. An updated list of the surveys of the Galactic polarized emission that have been conducted and being carried out can be found in Tables 1 and 2, respectively, in Landecker (2012), while a review of the radio polarization measurements from the beginning to the present day was presented by Wielebinski (2012). As an important by-product, it can be mentioned that these surveys together with the total intensity are the main source for identifying new SNRs. Recently, 79 SNRs have been observed during the Sino-German polarization survey of the Galactic plane performed with the Urumqi 25 m telescope at 6 cm (Han et al. 2014). Combining these data with observations made with the Effelsberg 100 m telescope at 21 and 11 cm, for the first time it was traced the magnetic field orientation for 23 out of the 79 sources observed and identified two new SNRs, G178.2−4.2 and G25.1−2.3.

5 Radio spectra

The knowledge of the spectral behavior of SNRs is vital to understanding particle acceleration at the shock fronts and the role of SNRs as factories of Galactic cosmic rays. The study of the global and spatially resolved radio-continuum spectra of SNRs provides significant constraints on shock acceleration theories. As mentioned in Sect. 2, in the case of strong shocks with a compression ratio of 4, DSA (diffusive shock acceleration) predicts for the radio flux density a spectral index $\alpha = 0.5$. However, when compared with the observed radio spectral indices, it is found that only 50 out of the 294 SNRs listed in Green (2014)'s catalogue have α between 0.5 and 0.6, a number that only increases to 65 if doubtful or poorly determined spectral indices are also considered. Figure 6 is an update of the summary of spectral indices presented by Reynolds (2011), after selecting the SNRs classified as shell type and separating those sources with well-known spectral index from those listed with a

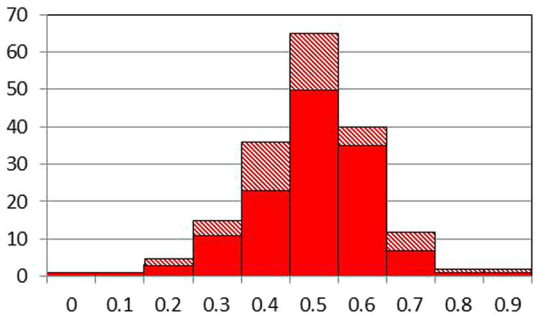

Fig. 6 Histogram of spectral indices of shell-type Galactic SNRs as extracted from Green (2014). The *solid bars* correspond to firm spectral index determination, while the *shadowed* ones to SNRs with uncertain spectral indices

question mark, for which a simple power law is not adequate to describe their radio spectra. The members of the composite and mixed-morphology classes are included as shell-type radio SNRs. It is worth mentioning that among the SNRs classified as shell type, almost 44 % have poorly determined spectra, with a percentage as high as 54 % for sources located in the fourth Galactic quadrant, very likely due to observational selection effects. These numbers, however, have to be considered with caution as the tabulated spectral indices in Green's catalogue come from very diverse studies, with a wide range of (uncatalogued) errors.

Nevertheless, the fact that less than one-fourth of the catalogued Galactic SNRs have the theoretically expected spectrum poses a problem to theorists. Different explanations have been proposed to address this. For instance, flatter spectra for increasing energy can be produced by shocks with low Mach number. The drawback of this hypothesis is that only a few SNRs would be expected to have such slow shocks, not enough to explain all the observed cases (Reynolds 2011). Also, second-order Fermi (stochastic) acceleration can play a role (Ostrowski 1999) and nonlinear shock acceleration (when accelerated particles influence the shock dynamics) can also produce flatter spectra (Ellison and Reynolds 1991; Reynolds and Ellison 1992).

Another important aspect to note is that theory predicts that the particle acceleration must be very efficient in young SNRs, corresponding to free expansion and especially early Sedov phases of evolution. This effect should translate into flatter spectra ($\alpha \leq 0.5$) for young SNRs. However, observations show that young SNRs have steeper indices (e.g. $\alpha = 0.77$ for Cas A, 0.58 for Tycho's SNR, 0.6 for SN1006, and about 0.8, with extreme values in the range 1.1–0.3 for the remaining of SN1987A.

In addition, the spectra of SNRs frequently show departures from a power law at the lower radio frequency extreme due to extrinsic or intrinsic processes that modify the electron energy distribution or the radio propagation. Three different physical processes that can affect the low radio frequency extreme have been proposed. They are: thermal absorption, synchrotron self-absorption, and the "Tsytovitch effect". Thermal absorption occurs when the non-thermal SNR radiation traverses a region with thermal plasma, producing a low-frequency turnover in the spectrum. Synchrotron self-absorption takes place if the intensity of synchrotron radiation within the source becomes sufficiently high, then reabsorption of the radiation through the synchrotron mechanism may become important, modifying the spectrum at low frequencies. The Tsytovitch effect can only be important in sources with very small size and weak magnetic fields (see Moffet 1975, for details). Bell et al. (2011) proposed that the spectrum can either steepen or flatten depending on the angle between the shock normal and the large-scale upstream magnetic field.

To narrow the gap between theory and observations and understand the physical meaning of the spectra, it is important to get good spectral index maps of many SNRs expanding in different environments and, if possible, in different evolutionary stages, to compare young and old populations. The accurate radio spectral study of SNRs provides three different pieces of important information: (1) the *global index*, a key parameter to constraining particle acceleration theories as mentioned above, (2) the *curvature* of the spectrum, useful to test radiation mechanisms and also to separate intrinsic from extrinsic factors that may modify the spectrum, and (3) the existence of *local variations* within the remnant, that helps to localize the sites where particle

acceleration takes place, the possible existence of radio PWNe (especially useful for the search of radio counterparts of PWNe discovered in other spectral regimes, such as X- or γ-ray), and the presence of superimposed or embedded sources of thermal absorption.

Since intrinsic or extrinsic spectral variations are often subtle, an important key is obtaining a large enough leverage arm in frequency space to tease them out. In the spectral studies, it is essential to separate the contribution of three factors that usually overlap, hiding the investigated properties: the intrinsic characteristics of the explosions, the contribution of the environment, and observational selection effects often imposed by the type of instrument used to acquire the radio data. This last one is not a trivial issue, since interferometric observations can over-resolve the source, missing total flux information, but single dish observations that produce accurate total flux measurements often confuse SNRs with nearby objects. An additional related issue is the problem of the proper subtraction of background emission, a serious issue since low-intensity emission extending over large angular distances (usually close to the Galactic plane) can result in a substantial contribution to the flux density of large SNRs. When analyzing the available radio spectra of SNRs, it is evident that most remnants are represented by only a few data points with substantial error bars, especially at the lower frequencies. In what follows, we discuss the different techniques developed to overcome the various problems that can affect the spectral studies and some interesting results.

Global spectrum To accurately determine the global indices and their curvature, one technique is the T–T plot (Leahy and Roger 1998) that fits pixel by pixel a linear relation to the brightness temperatures measured at two frequencies, deriving a temperature index from the slope ($T_\nu = T_0 \nu^{-\beta}$, where $\beta = \alpha + 2$). To investigate the possible curvatures, three or more frequencies must be used taking pairs of maps. This procedure guarantees that the derived spectral index, either total or local, is not sensitive to differences in the zero levels between the maps at the two considered frequencies. In any case, it is important that the images to be compared have similar angular resolution and sensitivity, whatever the technique used to obtain the data (single dish, interferometers or both combined).

Kassim (1989) carried out a pioneer work of observing numerous SNRs of the first quadrant at low radio frequencies and compiled existing observations, producing an atlas of radio SNR spectra, finding that about 10 out of the 32 observed SNRs show turnovers at low radio frequencies (below $\sim$100 MHz), which was interpreted as due to the presence of a widespread, but inhomogeneous ionized absorbing medium along the line of sight, probably associated with the extended HII region envelopes (EHEs). Figure 7 shows an example of spectrum with low-frequency turnover (bottom) and two examples of broadband spectral energy distribution (SED) to illustrate the utility of the radio spectra to fit models to the γ-ray emission (upper).

Spatial spectral variations The study in radio wavelengths of spatial spectral variations inside an SNR can provide important information about the physical conditions of the interior plasma. One problem in the study of spectral variations across an SNR is the confusion with unrelated overlapping structures. To address this difficulty, Katz-

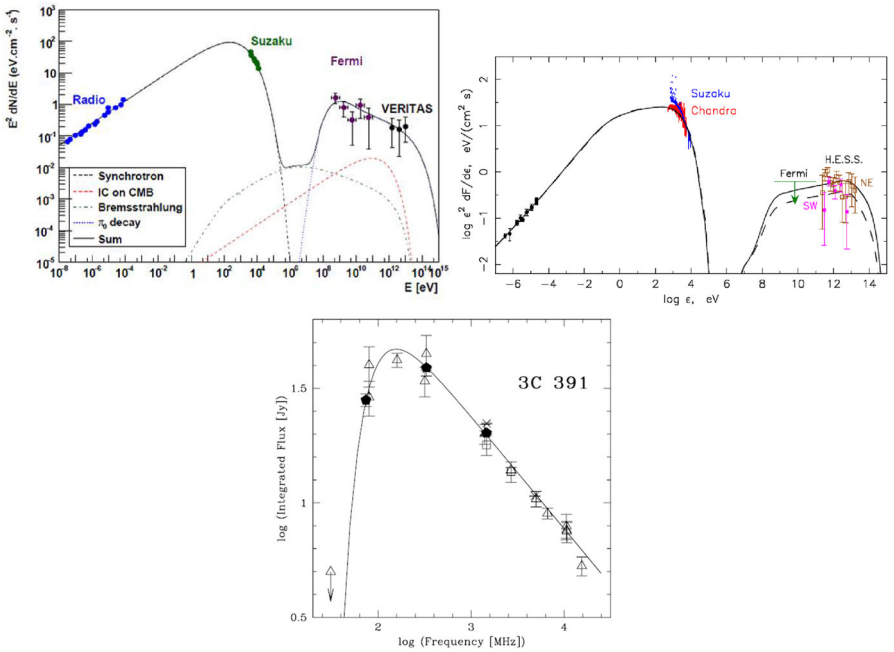

Fig. 7 *Upper* broadband spectral energy distribution from radio to γ-ray showing the importance of the radio data to fit models in Tycho SNR (*left* from Giordano et al. 2012) and in SN1006 (*right* from Berezhko et al. 2012). *Bottom* radio continuum spectrum for SNR 3C 391 showing a turnover in the spectrum at frequencies $\leq$100 MHz, indicative of free-free absorption from thermal ionized gas along the line of sight (from Brogan et al. 2005)

Stone and Rudnick (1997) developed the tomographic technique, designed to isolate structures with different spectra. Spectral tomography involves making a gallery of maps using different test α, in which each tomographic image between frequencies ν_1 and ν_2 is $I_t(\alpha_{\rm test}) = I_1 - (\nu_1/\nu_2)^{\alpha_{\rm test}} I_2$. Features or regions which have a spectral index identical to the test value will vanish in the tomographic map. Spatial components that have different spectral indices will appear as positive or negative features depending upon whether the spectrum is steeper or flatter than the assumed test value. This method has been successfully applied to analyze spatial spectral variations, for example in the SNRs of Tycho (Katz-Stone et al. 2000), Kepler (DeLaney et al. 2002), G292.0+1.8 (Gaensler and Wallace 2003), and in Puppis A (Castelletti et al. 2006). The method is particularly useful to locate small-scale spectral variations, providing a more accurate picture than the simple comparison between images at different frequencies. Figure 8 shows the tomographic image obtained for Puppis A for $\alpha_{\rm test} = 0.6$, where it can be noticed a spectral pattern formed by short horizontal, almost parallel fringes with α alternatively steeper and flatter than the background, reproducing the "wave-like" morphology observed in the total power image along the NE, NW, and S borders of Puppis A.

A significant breakthrough occurred with the first spatially resolved detection of thermal absorption towards the SNR 49B (Lacey et al. 2001), helping to explain

Fig. 8 Tomographic image of Puppis A from Castelletti et al. (2006) for $\alpha_{\rm test} = 0.6$. *Bright regions* have α steeper than $\alpha_{\rm test}$, while *dark regions* correspond to α flatter than $\alpha_{\rm test}$

the long mysterious presence of radio recombination lines towards this non-thermal source.

Soon after, a number of additional cases of resolved thermal absorption came to light, as for example the observation of a cocoon of thermal material in the SNR 3C391, marking the ionized boundary of the interaction of an SNR with a neighbouring molecular cloud (Brogan et al. 2005).

Another interesting example is the detailed spatial spectral study performed on Cas A, where Kassim et al. (1995) showed that the data were consistent with absorption by ionized gas inside the radio shell, probably related to unshocked ejecta still freely expanding within the boundaries of the reverse shock as delineated by X-ray observations. DeLaney et al. (2014) extended these observations and their analysis to constrain the physical properties of a component of SNRs that has been heretofore very difficult to study.

The spectral study carried out by Castelletti et al. (2011a) in IC443 revealed the existence of two different spectral components, both with flat spectrum ($\alpha \leq 0.25$) but of distinct origin, one extrinsic and the other intrinsic. One of these components coincides with the brightest parts of the remnant along the eastern border and perfectly matches the region where ionic lines are detected in the J and H infrared bands. Such correspondence is the manifestation of the passage of a J-type shock across an interacting molecular cloud that dissociated the molecules and later ionized the gas. This ionized gas produces thermal absorption along the line of sight, resulting in the observed flattened spectrum. The other flat spectrum component is more fragmented and located near the center of the SNR, in spatial coincidence with a region with a molecular cloud and γ-ray emission (Fig. 9), suggesting that the origin in this case is the particle acceleration that takes place at the shock front.

6 Distances to SNRs

A precise estimate of the distance to SNRs is essential to determine the physical parameters and understand their nature. It is, unfortunately, one of the most diffi-

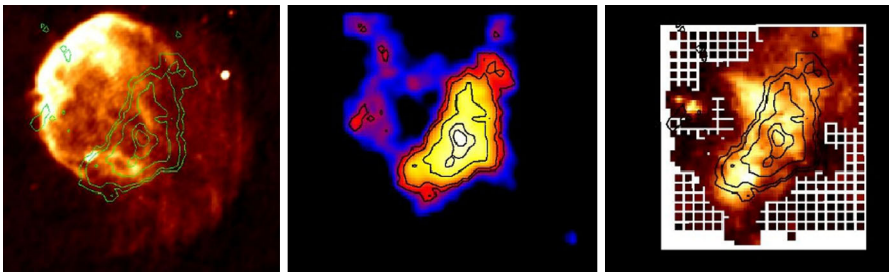

Fig. 9 The SNR IC443: *left* radio-continuum at 330 MHz (in *greys* from Castelletti et al. 2011a) with γ-ray emission from VERITAS (*contours*); *middle* VERITAS image of very-high-energy (VHE, $E \geq 100$ GeV) γ-ray emission (Acciari et al. 2009); *right* molecular CO emission (in *greys* from Zhang et al. 2010, with γ-ray emission overlapped in *contours*)

cult quantities to measure with accuracy. Wilson (1970) expressed that "At present, distances to only a few SNRs are known with any reliability. Optical estimates are restricted to those SNRs which are rather near the Sun and, while nearly one hundred SNRs have been found (Milne 1970), distance estimates independent of any theory of SNR evolution are available for only a few sources". Today, more than four decades later, the situation has scarcely improved and only one-third of the catalogued Galactic SNRs have a distance estimate, several of them with large uncertainties or barely expressed as limits.

The most precise determinations come from the combination of measurements of different independent quantities. Trimble (1973) addressed the distance calculation for the Crab Nebula using 12 different lines of evidence through methods depending on the dynamics of the nebular expansion, on physical processes in the supernova or the remnant, and involving the properties of the interstellar medium between us and the nebula or the pulsar. This was an exceptionally well-studied case, and yet today it is affirmed that the true distance of Crab Nebula remains an open question owing to uncertainties in every method used to estimate its distance and the error amounts to 25 % ($d = 2 \pm 0.5$ kpc).

In general, for less famous sources, several methods have been used to measure distances to Galactic SNRs, including the $\Sigma - D$ (radio surface brightness-to-diameter) relation, kinematic distances through atomic and molecular absorption and emission, association with other objects with known distances (usually HII regions, OB associations, pulsars) assuming that they are neighbours, X-ray and optical observations, etc. Each approach has its advantages and disadvantages, briefly discussed in what follows.

$\Sigma - D$ relation Although the application of this method is very controversial, it is described for its historical value and because in some cases it may provide a first guess when no other distance indicator is available. It is only applicable to shell-type SNRs. The basic assumption is that since at a first approximation Σ_ν, the mean radio surface brightness at frequency ν can be assumed as an intrinsic property of the SNR, it is a distance-independent observational parameter (Shklovsky 1960a, b). The first theoretical $\Sigma - D$ relation was derived by Shklovsky (1960a) and the first empirical relations were derived by Poveda and Woltjer (1968). Clark and Caswell (1976)

describe that after reaching a maximum value shortly after the birth of the supernova, it may be expected that Σ decreases monotonically with time, while the outer linear diameter, D, of the expanding SNR will increase monotonically with time. The basic idea is then to construct an empirical $\Sigma - D$ relation using calibrators with distances known by other methods. It is expected that there would not be too much scatter in this "evolutionary track". For the relation $\Sigma_\nu = AD^\beta$, the distance is derived as $d \propto \Sigma_\nu^{1/\beta}\theta^{-1}$, or, in terms of observable quantities, $d \propto S_\nu^{1/\beta}\theta^{-(1+2/\beta)}$, where S_ν is the flux density at the observing frequency ν and θ is the angular diameter of the remnant. This formula also assumes that the SNR boundary is circular; when this is not the case, it is commonly defined an equivalent diameter as $\theta = 2\sqrt{\text{area}/\pi}$. As mentioned, departures from sphericity are not uncommon, as they depend on environmental conditions and/or the orientation of the observer relative to the source. The ellipticity of typical remnants suggests that the variation of mean apparent angular diameter with orientation is sometimes as great as 10 %.

The reliability of this method has been seriously questioned, since there is no theoretical basis for a single equation to cover the evolution of SNRs over their whole lifetime and expansion in a variety of ambient media (see discussions in Green 1984, 1991). Evolutionary paths may differ substantially from one SNR to another, since they come from different stellar progenitors, probably experienced explosions with distinct physical characteristics, and may be expanding in interstellar media with a wide range of densities, from the evacuated interior of a wind-blown bubble, to a dense molecular cloud. However, in spite of the serious objections, this method has been widely applied for years and there have been several attempts to improve it in different ways. The distances of the sources used as calibrators were refined by changing the kinematical estimates through the application of a more modern rotation curve for the Milky Way, by taking new data from associations of SNRs with pulsars or molecular clouds, or by comparing with new X-ray and optical data. The different estimated power law index β varies in the range -2.38 to -5.2 (see Case and Bhattacharya 1998, for a summary and comments on the different calibrations). Pavlovic et al. (2014) presented the most recent fitting based on a revised calibration sample consisting of 65 Galactic SNRs, deriving $\beta = -5.2$. Arbutina et al. (2004) showed that the only case where a single $\Sigma - D$ correlation could be established was for the SNRs in the starburst Galaxy M82, and suggested that a similar behaviour could exist for a sample of Galactic SNRs associated with large molecular clouds. They conclude that the density of the environment is probably a crucial parameter to regulate the diameter during SNR evolution.

Kinematical method Basically, this method is based on the construction of an absorption HI spectrum by subtracting an average spectrum obtained from an area projected against a region with strong continuum emission of the target SNR, from a spectrum, or average spectrum, of an adjacent background region. Using the radial velocity of the absorption peak and by applying a Galactic circular rotation model[4] to convert radial velocities into distances, it can be set a distance, or range of acceptable distances, for the SNR. Complications arise when the HI emission is patchy and cause spurious

[4] Updated models for the Milky Way are presented in Bhattacharjee et al. (2014).

absorption features or when the continuum is faint and it is not possible to construct acceptable absorption spectra, with peaks noticeable at least at a 5-σ level. Tian and Leahy (2008) apply a combination of HI absorption plus CO emission to overcome some of the basic problems. Kinematical distances can also be derived from the study of the ISM around the SNR. When there is evidence of interaction between the SNR and the surrounding atomic or molecular gas (Sect. 7), the radial velocity at which the best signature is identified can be used to establish an approximate distance to the SNR.

However, even when the radial velocity of the absorption or emission associated feature is clearly defined, there still exists the problem of the ambiguity of the Galactic rotation curve within the solar circle, i.e. for each radial velocity, there are two corresponding distances equally spaced on either side of the tangent point. Moreover, although with the help of other indicators a single distance can be established, the circular rotation model still adds large intrinsic uncertainties (the model holds only for low Galactic latitudes and ignores systematic stream motions in the Galaxy, rolling motions in the Galactic arms, random cloud velocities, etc.) and the distances derived using kinematical methods have intrinsic (inherent to the method) uncertainties greater than $\sim$25–30 %.

Distances derived from X-ray observations Kassim et al. (1994) proposed a formula for shell-type SNRs to estimate distances in the cases where it can be assumed that the SNR shell is in the adiabatic expansion phase, that the measured X-ray temperature gives a reliable estimate of the SN shock velocity, and that an initial energy of the order of $E_0 \sim 10^{51}$ erg is valid for all SNe. In these cases, the distance to an SNR could be derived as a function of the initial energy, the observed angular diameter of the SNR shell, the measured X-ray flux corrected for interstellar absorption, the thermal temperature of the X-ray emitting gas, plus a function that describes the power emitted by hot electrons in a low-density plasma via free-free emission (that depends on both the energy band of the emission and the temperature of the plasma) as $D_s = 8.7 \times 10^6 \epsilon_0^{0.4} P(\Delta E, T)^{0.2} \theta^{-0.6} F_{X_0}^{-0.2} T^{-0.4}$. The method was applied to a sample of SNRs detected with ROSAT, with the major uncertainty related to the basic physical assumptions rather than to measurement errors.

Other application of X-ray data to constrain the distances to SNRs was for example the one used in the study of the SNR RX J1713.7-3946 (G347.3−0.5) (Cassam-Chenaï et al. 2004). The procedure consists of plotting the cumulative absorbing column calculated from atomic and molecular gas observations as a function of the radial velocity and comparing with the absorbing column NH as derived from a fit to the X-ray data. The radial velocity at which these quantities are equal is later translated to distance through a kinematic model of Galactic rotation.

In summary, the distances estimated for SNRs have to be considered with caution. Even in the best cases when more than one independent distance determination can be used, the derived distances are still imprecise, either because of observational inaccuracies or because of doubtful assumptions involved in the formulae used to calculate them.

7 Interaction of SNRs with the surrounding ISM

The interaction between the strong SN blast wave and the surrounding interstellar medium has profound consequences on the remnant as well as on the gaseous interstellar matter. SN explosions are the main sources of chemical enrichment of the ISM, while the distribution and physical conditions of the surrounding gas represent the primary physical constraint to the expansion of the SN shock. The investigation of the SNR/ISM interaction is not only necessary to improve our knowledge of SNRs, but also to understand the response of the interstellar gas to the enormous injection of energy and momentum that an SN explosion represents. Additionally, as already mentioned in Sect. 6, the identification of physically associated interstellar gas serves to calculate the kinematical distance to the remnant. The study is also very important to understand the production of γ-rays and hence the role of SNRs powering Galactic cosmic rays, as clouds illuminated by the protons accelerated in a nearby SNR could be bright γ-ray sources (e.g. Aharonian and Atoyan 1996; Berezhko and Völk 2000; Gabici et al. 2009; Butt 2009; Ellison and Bykov 2011).

The ISM is formed by various components in different physical conditions. It is arranged in a variety of structures and phases, including big complexes of dense clouds, hot bubbles, sheets, walls, filaments, etc. (e.g. Lequeux 2005; Cox 2005). Some of these structures are directly created by the SNe and SNRs. The environmental characteristics play a crucial role in the shape, energetics, temporal evolution, and destiny of SNRs. Before analyzing the consequences of the mutual interaction between SNRs and the ISM, in what follows we briefly review the basic characteristics of the ISM in our Galaxy.

Phases of the interstellar medium:

- *The molecular medium (MM)*, characterized by cold dense molecular clouds which are mostly gravitationally bound, with typical temperatures $\leq$100 K, volume densities $\geq 10^3$ cm^{-3}, and volume filling factor $f \leq 1\,\%$. A mass of about 1.5×10^9 $M_\odot$ of molecular gas is distributed predominantly along the spiral arms of the Milky Way, occupying only a very small fraction of the ISM volume and within a narrow midplane with a scale height $Z \sim$50–75 pc.
- *The cold neutral medium (CNM)*, distributed in rather dense filaments or sheets, with typical temperatures of $\sim$100 K, volume densities $\sim$20–25 cm^{-3}, and volume filling factor f $\sim$2–4 %. This phase is most readily traced by HI measured in absorption.
- *The warm neutral medium (WNM)*, which provides the bulk of the HI seen in emission, with typical temperatures $\geq$6000 K, volume densities $\sim$0.3 cm^{-3}, and volume filling factor $f \geq 30\,\%$.
- *The warm ionized medium (WIM)* with $T \sim$8000 K, $n \sim$0.03–0.3 cm^{-3}, and $f \geq 15\,\%$, ionized gas associated with HII regions, but also diffuse filling a considerable fraction of the ISM.
- *The hot ionized medium (HIM)* with $T \sim 10^6$ K, $n \sim 10^{-3}$ cm^{-3} and $f \leq 50\,\%$. This phase of hot gas is produced by supernova explosions, has a long cooling time and consequently a large fraction of the ISM is filled with this "coronal" gas.

It can be viewed as the accumulated superposition of dissipated SNRs interiors integrated over the lifetime of the Galaxy (McKee and Ostriker 1977).

The cold, warm and hot phases are in global pressure equilibrium, while the molecular material is mostly confined to clouds which are held together by gravitation. The filling factor for each of the phases is highly uncertain, as is the topology of the ISM. In general, the ISM has structures on all scale lengths, from smaller than 1 pc to larger than 1000 pc. Through HI observations of the Galaxy, it has been known that the ISM is pervaded by holes surrounded by shells and supershells (Heiles 1984; McClure-Griffiths et al. 2002; Suad et al. 2014), as a result of individual or collective action of stellar winds of massive stars and supernova explosions. The interior of these bubbles is filled with HIM.

Molecular gas, on its side, is mostly (∼90 %) assembled in massive structures distributed in large clumps (GMCs, the giant molecular clumps with masses of $\sim 10^4$–10^6 $M_\odot$, diameters ∼50 pc, and average densities n_{H_2} ∼100–300 cm^{-3}), clouds (M $\sim 10^4$ $M_\odot$, diam ∼5 pc, n_{H_2} ∼300 cm^{-3}), and condensed cores (possible birth sites of new stars, with M $\sim 10^3$ $M_\odot$, diam ∼2 pc, n_{H_2} $\sim 10^3$ cm^{-3}) (e.g. Williams et al. 2000). They are principally composed of molecular hydrogen and dust and, in very little quantities, by some of the ∼140 molecular species that have been identified in interstellar or circumstellar gas.

7.1 Consequences of the interaction

As expected, the expanding SNR shock front undergoes a different evolution according to the phase of the ISM that it encounters in its expansion, and the dynamical evolution of an SNR is modified with respect to the simple description presented in Sect. 2. Given a constant pressure in the SNR and that the postshock pressure scales with $\rho_0 v_s^2$ (where ρ_0 is the ambient density and v_s the shock velocity), it is expected that the SN rapidly expands in the lowest density phase, while dense clouds are slowly crushed by lower velocity shocks. The energy can be conducted from the hot gas filling the SNR to embedded clouds, leading to their evaporation. A complete treatment of the expressions that govern the expansion of an SNR in these cases can be found in Tielens (2005). In the end, the exchange of mass, energy, and momentum between the different phases govern the dynamical evolution of the SNR, and the appearance of the SNR in the different spectral regimes reflects the structure of the surrounding medium.

Due to the short lifetimes of massive stars, most core-collapse SNe (resulting from explosions of types SNII, SNIb and SNIc) are located close to the molecular concentrations where the precursors were born. Therefore, a large percentage (as high as ∼75 %) of the Galactic SNRs are expected to interact with MCs. One important consequence of these interactions is that because of the compression and high temperatures of the SNR shocks propagating inside MCs, some chemical reactions otherwise not possible can occur, creating new molecular species (e.g. Tielens 2005). For example, a recent work by Dumas et al. (2014) reported the detection of SiO emission triggered by the passage of the W51C SNR shock.

Slane et al. (2015) describe the X-ray and γ-ray signatures of the interaction of SNRs with molecular clouds and summarize the different criteria that can be used

to establish the existence of a physical relation between an SNR and a cloud seen in projection against the remnant. To unambiguously establish whether an SNR is physically associated with an interstellar cloud, removing confusion introduced by unrelated gas along the line of sight, is not trivial and usually requires several distinct criteria to demonstrate physical interaction. Basically, morphological traces along the periphery of the SNRs, such as arcs of gas surrounding parts of the SNR, or indentations in the SNR outer border encircling dense gas concentrations. Usually, such features indicate that a dense external cloud is disturbing an otherwise spherically symmetric shock expansion. These initial signatures need to be confirmed with more convincing, though more rare, features like broadenings, wings, or asymmetries in the molecular lines spectra (Frail and Mitchell 1998), high ratios between molecular lines of different excitation state (Seta et al. 1998), detection of near infrared H_2 or [Fe II] lines (e.g. Reach et al. 2005), peculiar infrared colors (e.g. Castelletti et al. 2011a), and the presence of OH (1720 MHz) masers. These masers were originally detected by Goss and Robinson (1968) in some SNRs, but their importance as proof of SNR/MC interaction was only recognized almost 30 years later (Claussen et al. 1997; Frail and Mitchell 1998), and their detection became the most powerful tool to diagnose SNR/MC interaction. In addition to being an ideal tracer of interaction, observations of OH (1720 MHz) masers provides an accurate estimate of the magnetic field intensity of the postshock gas in SNRs via Zeeman splitting (e.g. Brogan et al. 2000).

Based on a combination of different techniques, Jiang catalogued a list of ∼70 Galactic SNR candidates to be physically interacting with neighbouring MCs,[5] of which 34 cases were confirmed on the basis of simultaneous fulfilment of various criteria, 11 were probable, and 25 were classified as possible and deserve more studies (Chen and Jiang 2013).

The basic method of investigating cases of SNR/ISM interaction is to survey the interstellar medium in a field around the SNR using different spectral lines, from the cold, atomic hydrogen emitting at λ21 cm to the dense, shielded regions of molecular hydrogen emitting lines in the millimetric and infrared ranges. The molecular gas is frequently studied through CO observations (usually the transition $^{12}C^{16}O$ J: 1–0 at λ 2.6 mm), since this molecule radiates much more efficiently than the abundant H_2 and can be detected easily. Later, the observed CO intensity has to be converted into total H_2 gas mass. According to the standard methodology, a simple relationship can be established between the observed CO intensity and the column density of molecular gas, such that $N(H_2) = XCO \times W(CO\ J: 1–0)$, with the column density, $N(H_2)$ in cm^{-2} and the integrated line intensity W(CO) in K km s^{-1}. Bolatto et al. (2013) present a complete review of the theory, techniques, and results of efforts to estimate XCO, the "conversion factor" from CO into H_2 in different environments. In the Milky Way disk, the representative XCO values varies between 0.7 and 2.8 $\times 10^{20}$ cm^{-2} (K km $s^{-1})^{-1}$ depending on the technique applied for the estimate. A value $XCO = 2 \times 10^{20}$ cm^{-2} (K km $s^{-1})^{-1}$ with 30 % uncertainty is recommended by Bolatto et al. (2013).

[5] http://astronomy.nju.edu.cn/~ygchen/others/bjiang/interSNR6.htm.

In HI (absorption and emission methods), numerous studies around SNRs have been carried out using single-dish and interferometric radiotelescopes, looking for traces of disturbances in the interstellar gas distribution caused by the SNR or its stellar progenitor (e.g. Dubner et al. 1998; Reynoso et al. 1999; Giacani et al. 2000; Velázquez et al. 2002; Koo and Kang 2004; Paron et al. 2006; Leahy and Tian 2008; Lee et al. 2008; Park et al. 2013). An interesting approach using atomic gas studies was recently used in the historic remnant of SN 1006 by Miceli et al. (2014), where an important connection between shock–cloud interaction and particle acceleration was demonstrated based on the comparison of X-ray with HI data.

Many dedicated studies were conducted towards several Galactic SNRs in different molecular transitions (e.g. Reach and Rho 1999; Moriguchi et al. 2001; Dubner et al. 2004; Moriguchi et al. 2005; Reach et al. 2005; Jiang et al. 2010; Paron et al. 2012; Li and Chen 2012; Hayakawa et al. 2012; Fukui et al. 2012; Gelfand et al. 2013; Kilpatrick et al. 2014, etc.). Of particular importance have been the molecular gas investigations around the SNRs IC443, W28 and W44, which have been the subject of many observational studies. These were the first SNRs where the OH (1720 MHz) masers were observed. In recent years, these sources became especially notorious as they are good examples of Galactic γ-ray sources detected in the TeV range as seen by H.E.S.S. and other Cerenkov telescopes, and in the GeV range by the Fermi and AGILE satellites.

The SNR IC443 (G189.1+3.0), because of its location in a relatively confusion-free region of the outer Galaxy, is a textbook case to analyze shock chemistry, and as such it has been thoroughly studied in many molecular transitions. From the first identification by Cornett et al. (1977), tens of works investigated the chemical and physical transformations introduced by the strong SNR shocks on the surrounding molecular clouds (see Kilpatrick et al. 2014, for an updated summary of molecular studies towards IC443). The morphology consisting of two semi-circular shells with different radii is an indication of expansion in an environment with a marked density contrast. IC443 is also an excellent example where the interaction of the SNR with a molecular cloud probably gave origin to the γ-ray emission through a hadronic mechanism. In effect, an excellent concordance was demonstrated by Castelletti et al. (2011a) by confronting the VERITAS very high energy γ-ray radiation (Acciari et al. 2009) with the ^{12}CO J = 1–0 cloud (Zhang et al. 2010) (Fig. 9), and the region where the radio-continuum emission of IC443 shows flat spectral indices not caused by thermal absorption (see Sect. 5).

The SNR W44 (G34.7−0.4) (Fig. 10) is another Galactic remnant whose interaction with a cloudy ambient medium has been deeply investigated, at first motivated by its morphology of a rather distorted shell with a significant flattening along the eastern edge, suggesting an encounter with dense ambient medium. Since the first HI study by Sato (1974), reporting the presence of a dense cold cloud in coincidence with W44, many observations have been performed in different molecular and IR lines (e.g. Dickel et al. 1976; Wootten 1977; Seta et al. 2004; Paron et al. 2009; Sashida et al. 2013; Anderl et al. 2014, and references therein). The IR data showed that this SNR expands in a dense medium with $n \sim 100$ cm^{-3} (Reach et al. 2005). Giuliani et al. (2011) used constraints set by CO data from the NANTEN Observatory, the radio spectrum as obtained by Castelletti et al. (2007), and optical data reported by

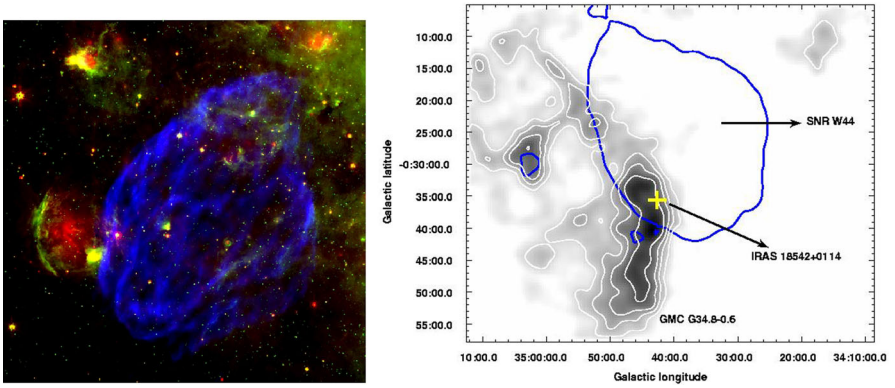

Fig. 10 *Left* radio continuum emission of the SNR W44 at 324 MHz (VLA image, in *blue*) with the infrared emission in the SNR region from *Spitzer* data at 8 μm (in *green*) and at 24 μm (in *red*) (from Castelletti et al. 2007). The *yellow spot* in the southeast corresponds to the HII region G034.8−0.7, an area where there is active star formation. *Right* ^{13}CO J = 1–0 distribution showing the giant molecular cloud GMC G34.8−0.6 interacting with the SNR W44. The cross shows the position of the infrared source IRAS 18542+0114. The *blue contours* trace the silhouette of SNR W44 displayed in Galactic coordinates (from Paron et al. 2009)

Giacani et al. (1997), to demonstrate that the γ-ray emission detected with AGILE in the energy range 400 Mev–3 GeV was consistent with hadron-dominated models. The possibility of star formation in the region of strong interaction between the expanding SNR shock and the adjacent molecular cloud (where there are IR sources with spectral characteristics of young stellar objects) is discussed below in Sect. 7.2.

Another interesting observational example of interaction can be found in the SNR Puppis A (G260.4−3.4), where CO and HI observations carried out by Dubner and Arnal (1988) first revealed that the SNR is expanding in an inhomogeneous environment, with clouds towards the east and northeast borders. Later, Reynoso et al. (1995) explored this SNR in HI with high angular resolution using the VLA (Fig. 11 left) revealing the distribution of a pre-existing interstellar HI cloud closely following the borders of the SNR shell as seen in X-rays. Inside the SNR, Hwang et al. (2005) investigated through X-ray images and spectra the most prominent spots of cloud–shock interaction (mainly the bright eastern knot, known as the BEK), revealing what has been the first X-ray identified example of a cloud–shock interaction in an advanced phase. From new CO observations, Paron et al. (2008) showed evidence of what has been left of the molecular clump engulfed by the SN shock and that currently evaporates emitting X-rays. Another interesting conclusion is that to the eastern boundary where the atomic gas is in touch with the SNR, the molecular emission is detached, indicating that the precursor radiation has dissociated the molecules of the adjacent cloud. It is also noticeable from Fig. 11 right that in X-rays, Puppis A has a "cellular" filamentary structure with a honeycomb appearance, confirming that it expands in a rich and complex environment. In addition, Fig. 11 right, showing the location of the radio border running outside of the sharp X-ray and IR limbs, is clear evidence that the radio radiation is the best indicator of the true position of the shock front.

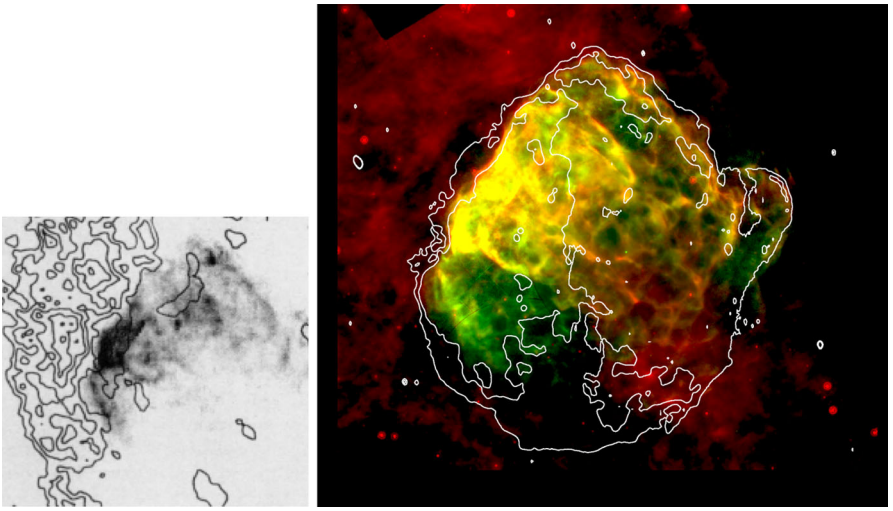

Fig. 11 *Left* distribution of the HI emission (in *contours*) around the SNR Puppis A, overlapping the ROSAT X-ray emission (in *greys*) as taken from Petre et al. (1982). Image extracted from Reynoso et al. (1995). *Right* two color image of Puppis A comparing the *Chandra* and *XMM-Newton* X-ray emission in the 0.7–1.0 keV band (in *green*) (Dubner et al. 2013), with IR emission as observed with Spitzer at 24 μm (in *red*) (Arendt et al. 2010). The *white contours* show radio-continuum emission at 1.4 GHz (from Castelletti et al. 2006)

7.2 Can SNRs trigger the formation of new stars?

Since Opik (1953)'s early idea that "the death of a star in a supernova explosion may lead to the birth of a great number of new stars", predicting that a ring of newborn stars would condense out of the expanding shell, it became a paradigm that one of the consequences of SNR/ISM interactions can be the formation of new stars. Vanhala and Cameron (1998) carried out numerical studies, concluding that shock waves with velocities in the range of 25–40 km s^{-1} are capable of triggering collapse in molecular cores immersed in clouds interacting with SNRs. Melioli et al. (2006) set constraints on the SNR radius and molecular gas density for which star formation is allowed. If the SNR–cloud interaction is too strong, the cloud is completely destroyed; if it is too weak, the molecular core never collapses. In summary, the theoretical conclusion is that if favourable conditions are given, triggered star formation can occur as a consequence of SNR/ISM interaction.

Wootten (1978) conducted one of the very first searches of star formation triggered by an SNR. From the analysis of an infrared object in a cloud near the SNR W44, the author concluded that it was an evidence of star formation stimulated by the expansion of the SNR. Since then, several searches have been carried out, including one based on multi-wavelegth data towards W44, where Paron et al. (2009) demonstrated that star formation was related to the nearby HII region G034.8−0.7 and not to the SNR. Other SNRs interacting with molecular clouds with indicators of active star formation have also been investigated, including W30 (Ojeda-May et al. 2002), G54.1+0.3 (Koo et al. 2008), G357.7+0.3 (Phillips et al. 2009), IC443 (Odenwald and Shivanandan 1985;

Xu et al. 2011), G18.8+0.3 (Dubner et al. 2004; Paron et al. 2012), etc. In all cases, even when the location of protostellar objects and young stellar object (YSO) candidates immersed in shocked molecular clouds were very promising, after comparing the characteristic timescale of star formation with the age of the SNRs, the general conclusion is that the stellar formation started before the SN explosion.

Desai et al. (2010) carried out the most complete and homogeneous search for star formation related to SNRs by examining the presence of YSOs and molecular clouds in the environs of 45 SNRs in the Large Magellanic Cloud. After a very detailed analysis, based on different arguments (positions, densities, timescales, etc.), the conclusion is that there is no evidence of SNR-triggered star formation in the LMC.

In conclusion, star formation is frequently seen near supernova remnants, but such physical association does not necessarily imply a causal relationship. Massive stars that end their lives exploding as SNe are formed in clusters or OB associations where the formation of new stars may continue and propagate outward for a prolonged period of time. It is then not surprising that core-collapse SNe are near young stars in star-forming environments. But apparently, the SNR shocks result in an increment of turbulence that is not compatible with star formation. In fact, the agitation may be so violent that it disperses the material, hindering further star-forming activity. This is an important open field of research that demands further theoretical and observational studies.

8 Comparison of radio emission with emission in other spectral ranges

The emission in different spectral regimes traces material with different physical conditions. Briefly, optical filaments observed in most SNRs arise from shocked interstellar medium that is cooling radiatively, while in a few remnants the optical emission includes oxygen-rich filaments, fragments of nearly pure ejecta launched from the core of the progenitor star during its explosion, or can be dominated by Balmer lines when a fast shock (velocities higher than $\sim$200 km s^{-1}) enters into partly neutral interstellar gas. The thermal X-ray emission contains essential information regarding the temperature, composition, distribution, and ionization state of the material synthesized and ejected in SN explosions, and of the ambient matter swept up by the supernova shock. If the origin of the X-ray emission is synchrotron, then its study can set powerful constraints on the role of the SN shocks in the production of cosmic rays. Infrared emission mainly marks the location of shock-heated dust. In summary, the body of multispectral observations is not only useful to understanding the properties of the SNRs and their precursors, but also to explore the interstellar gas.

The search for a correlation between radio and IR emissions is a powerful tool for distinguishing thermal from non-thermal emission. The combination of the VLA survey of the Galactic plane at 330 MHz with the Midcourse Space Experiment (MSX) at 8μm served to discover 31 new SNRs and 4 candidates in the inner Galactic plane region, where the diffuse synchrotron emission and thermal HII regions cause more confusion. The SNRs are anti-correlated with dust emission, while HII regions are invariably surrounded by a shell of bright 8 μm emission (Brogan et al. 2006). Also, this methodology has been applied to provide accurate estimate of the integrated radio flux

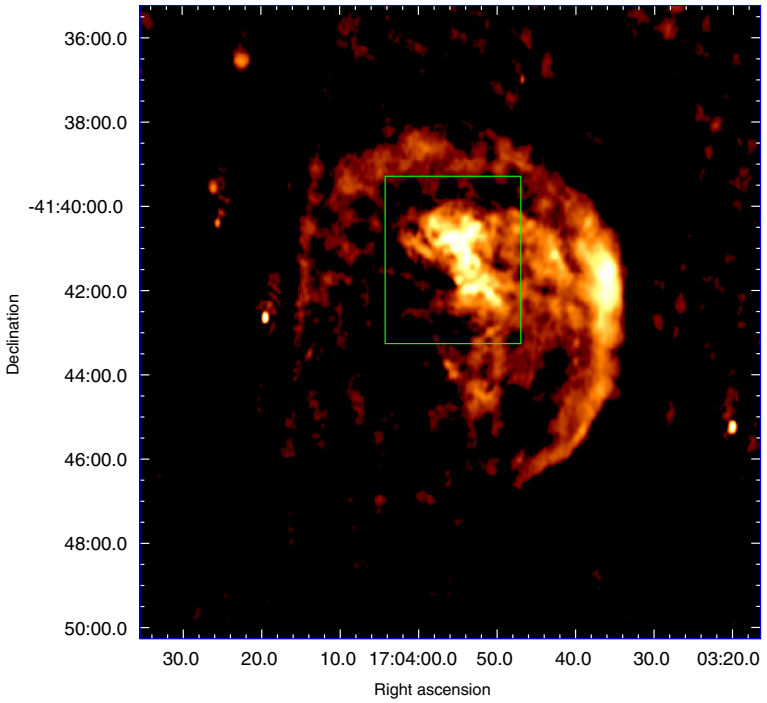

Fig. 12 Radio image of G344.7−0.1 at 1.4 GHz taken from Giacani et al. (2011). The *green square* shows the location of the radio nebula near the geometric center of the remnant

density in remnants located in complex regions of our Galaxy where the contamination with thermal structures is high, as for example in the SNRs RX J1713.7-3946 (Acero et al. 2009) and G338.3−0.0 (Castelletti et al. 2011b). Besides, the comparison with radio emission from SNRs has been one of the prime methods to identify the nature of several γ-ray sources detected in the GeV and TeV ranges (more than 20 Galactic TeV sources are related with SNRs).

Nowadays, the study of almost all SNRs is tackled from a multi-wavelength approach. In what follows, we describe some sources in which the comparison of radio emission with emission in other spectral windows unveiled interesting results.

G344.7−0.1 This SNR is a clear example where the comparison between radio, IR at 24 μm, and X-ray images elucidated the nature of a radio nebula located near the center of the remnant (Fig. 12). From a radio spectral study carried out in this region of the remnant using the Very Large Array (VLA, NRAO) and the Australia Telescope Compact Array (ATCA) data at 1.4 and 5 GHz, Giacani et al. (2011) determined a mean radio spectral index of $\alpha \sim 0.3$ for the nebula, a value compatible with those of radio PWNe. The combination of the emission in the three mentioned spectral ranges allowed the authors to rule out a PWN origin, concluding that the central bright radio feature is probably the result of strong shocks interacting with dense material. This interaction enhanced the infrared emission from shocked dust and favoured particle acceleration, resulting in a flatter radio spectrum.

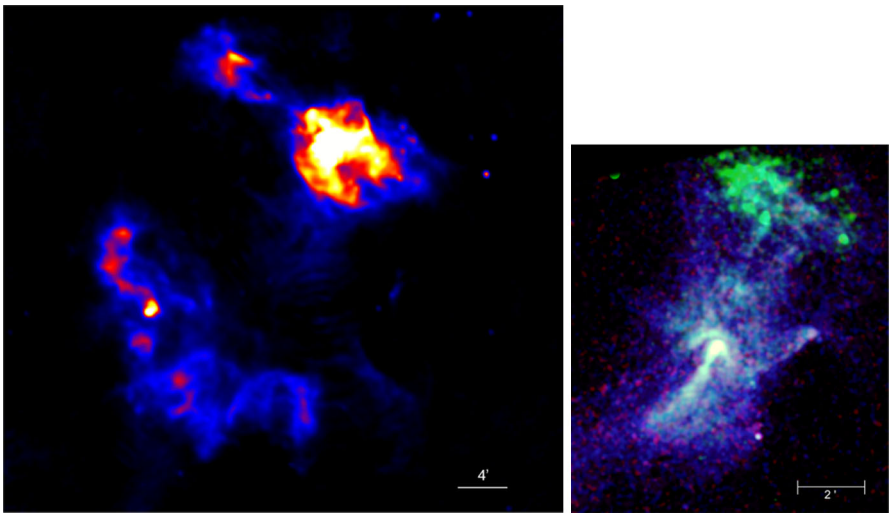

Fig. 13 *Left* radio continuum image of the SNR G320.4−1.2 at 1.4 GHz taken from Dubner et al. (2002). *Right* X-ray image by *Chandra* (Gaensler et al. 2002). Credit Image NASA/MIT/B. Gaensler et al.

G320.4−1.2 (MSH 15-52) A complex interacting system that has been observed throughout the electromagnetic spectrum is formed by the SNR G320.4−1.2, the energetic pulsar PSR B1509-58 and its PWN, and the HII region RCW 89 (Fig. 13). SNR G320.4−1.2 has an unusual radio appearance consisting of two distinct components: towards the northwest, a bright centrally concentrated source with a ring of radio clumps in coincidence with the optical nebula RCW 89, and towards the southeast a fainter partial shell (Fig. 13 left). The pulsar PSR B1509-58, detected in radio, X-rays, and in γ-ray, is located near the center of G320.4−01.2. In the X-ray domain, this system has a complex picture with a different morphology (Fig. 13 right). The emission is dominated by a jet-like structure emerging from the pulsar, the PWN, and extended emission, thermal in origin coincident with the northern radio component of the SNR and with the HII region RCW 89. Gaensler et al. (1999) proposed that this complex system can be explained as a result of a low-mass or high-energy explosion occurring near one edge of an elongated low-density cavity, which was confirmed by observations of the neutral gas in the region by Dubner et al. (2002). The pulsar appears to be generating twin collimated outflows, the northern part of which interacts with the SNR producing the collection of the clumps observed in the radio and the X-ray band. Gaensler et al. (2002) later reported the discovery of the long-sought PWN on the basis of comparison of new *Chandra* X-ray data with radio morphology.

G292.0+1.8 This remnant is another interesting source that has been subject to multi-wavelength observational campaigns. It is a textbook example because it has all the properties of a core-collapse SNR: a central pulsar (PSR J1124-5916) feeding a PWN, metal-rich ejecta, shocked CSM, and a blast wave. For a summary of previous observations, see Ghavamian et al. (2012). Briefly, it is characterized by a remarkable network of filaments seen in optical and X-rays, which are fragments of supernova

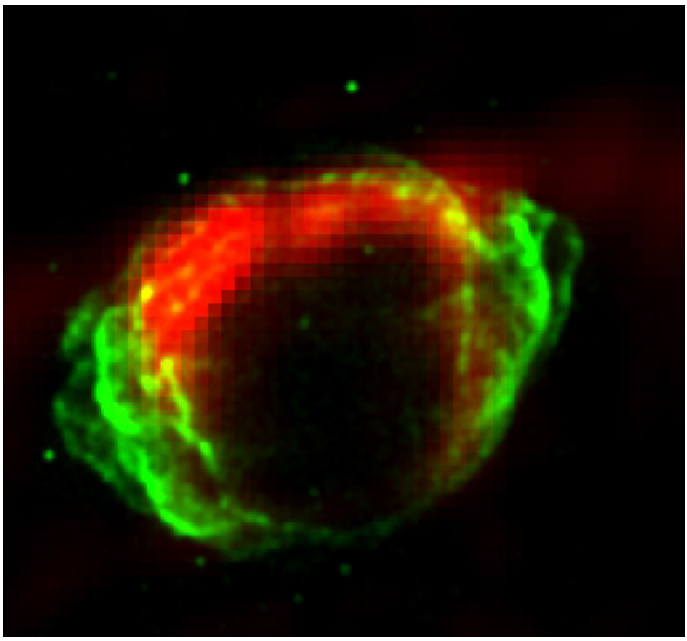

Fig. 14 *Chandra* image of G1.9+0.3 (in *green*) (Borkowski et al. 2013) superimposed with VLA radio image at 4.9 GHz (in *red*) as reprocessed from archival VLA data by the authors of this paper

ejecta (Winkler and Long 2006; Park et al. 2002, 2004, 2007). The X-ray image also reveals bright filaments running from east to west, named the "equatorial belt", probably shocks propagating in circumstellar material (Park et al. 2002). In the radio band, a mutifrequency study of the remnant performed with ATCA at 20, 13, and 6 cm by Gaensler and Wallace (2003) revealed the presence of a polarized and flat-spectrum bright central core, representing the radio PWN, surrounded by a circular fainter plateau with steep spectrum, which represents the SNR shell. Curiously, a series of radial filaments with much flatter spectrum are located over the plateau. The comparison with the X-ray emission allowed Gaensler and Wallace (2003) to propose that Rayleigh–Taylor instabilities near the SNR contact discontinuity originated the formation of such filaments (Fig. 3 in Gaensler and Wallace 2003).

G1.9+0.3 It is the youngest remnant detected in the Milky Way (age ∼150 years), opening as such the opportunity to study a Galactic SNR at its very early development. The morphology of G1.9+0.3 can be described as an almost complete shell in radio and in X-rays (Green et al. 2008; Reynolds et al. 2008), but the comparison between the distribution of the emission in both spectral ranges revealed a peculiar anti-correlation. While the radio remnant is clearly brighter along the northern border, the X-rays have a notable bilateral east–west symmetry including two extensions ("ears") not detected in the radio band (Fig. 14). It is one of the few shell SNRs with an X-ray spectrum dominated by synchrotron emission (Reynolds et al. 2009). But this is not the only origin of the X-ray emission. Borkowski et al. (2010) reported the presence of lines of Fe, Si, and S in small regions of the northern limb with spectroscopic velocities

of about 14 000 km s^{-1} and a line at 4.1 keV, identified as due to ^{44}Sc (the first firm detection of this element in an SNR). Based on the presence of Fe lines, high velocities, absence of PWN, and bilaterally symmetric non-thermal X-ray emission as in SN 1006, Borkowski et al. (2013) suggest a Type Ia origin for G1.9+0.3.

9 Supernova remnants in the Magellanic Clouds

The Magellanic Clouds are an ideal laboratory to investigate the properties, both global and individual, of SNRs across the whole electromagnetic spectrum. The facts that the distances are known (49 kpc for the LMC and 59 kpc for the SMC), that the LMC is nearly face-on, so that all remnants are nearly co-distant, and that even for the rounder SMC there is a range of only ±5 kpc with respect to the mean distance allow for accurate estimation of physical parameters of the remnants. At the same time, the proximity permits radio observations with good angular resolution, revealing the structure of individual objects and facilitating accurate multi-spectral comparisons.

One of the very first identifications of an SNR in the Magellanic Clouds was reported by Mathewson and Healey (1963) based on radio observations carried out with the 210 ft steerable reflector at the Australian National Radio Astronomy Observatory. It was followed by several searches using the Molonglo Observatory Synthesis Telescope (MOST) that permitted the identification of new members based on the combination of radio observations with optical and X-ray data. Mathewson et al. (1983) compiled a catalogue of SNRs in the Magellanic Clouds with 25 confirmed remnants in the LMC and 6 in the SMC. Later on, the search and studies of SNRs in our neighbouring dwarf galaxies took advantage of the Australia Compact Telescope Array (ATCA) that improved the angular resolution by factors between 5 and 35 compared with the best previously available radio data. Several works reported discoveries of new members and detailed studies of already known SNRs (e.g. Amy and Ball 1993; Manchester et al. 1993a, b; Dickel et al. 1993; Dickel and Milne 1995, 1998, etc.)

Badenes et al. (2010) compiled from the existing literature a catalogue of multi-wavelength observations with 77 confirmed SNRs in the Magellanic Clouds (54 in the LMC and 23 in the SMC), arguing that this list comprises a fairly complete record of SNe that exploded over the last ∼20 kyr. After Badenes published the catalogue, at least seven new cases were confirmed in the LMC (Grondin et al. 2012; Maggi et al. 2012; Kavanagh et al. 2013; Bozzetto et al. 2013; Maggi et al. 2014). Of all the 84 SNRs identified to date, only 4 of them (SNR J005.9-7310 in the SMC, and MC SNR J058-6830, MC SNR J0511-6759 and MC SNR J0517-6759 in the LMC) have not been detected in the radio band, possibly because they are old and faint (Maggi et al. 2014).

Badenes et al. (2010) carried out statistical studies of the SNRs in the Magellanic Clouds concluding that the size distribution of remnants is approximately flat with a cutoff at $r \sim 30$ pc. The authors propose that most of the SNRs are in the Sedov phase of evolution, quickly fading below detection as soon as they reach the radiative stage.

Among all SNRs in the Magellanic Cloud, the radio remnant of SN 1987A deserves special attention, because it offered the possibility of tracing in great detail its temporal evolution. In what follows, the main aspects of this source are summarized.

The radio remnant of the SN 1987A SN 1987A was the first naked-eye SNe event since the invention of the telescope. It exploded in 1987 February 23 in the Large Magellanic Cloud. Briefly, the progenitor of SN 1987A, Sk-69°202, with an initial mass estimated in $\sim$20 $M_{\odot}$, is believed to have evolved from a red supergiant (RSG) into a blue supergiant (BSG) approximately 2×10^4 years prior to the explosion (Crotts and Heathcote 2000). Optical imaging revealed a complex circumstellar medium (CSM) surrounding the explosion, consisting of a triple-ringed structure (Burrows et al. 1995, and reference therein). The two outer rings appear to be the cap of an hourglass-shaped structure enveloping the SN itself. The inner ring, also referred to as the equatorial ring, is believed to represent an equatorial density enhancement in the CSM, located at the interface between a dense wind emitted from an earlier red giant phase of the progenitor star and a faster wind emitted by the star in more recent times.

In the radio band, the emission from the SN 1987A was detected at 843 MHz with the MOST two days after the SN event. This emission reached its maximum value of around 140 mJy 4 days after the explosion and then decayed rapidly to become undetectable less than a year later (Turtle et al. 1987). This radio outburst has been explained as the consequence of the rapidly moving, low-density BSG wind, which produced only a short-lived period of radio emission when hit by the SN shock (Storey and Manchester 1987; Chevalier 1998).

Approximately 1200 days after the explosion, radio synchrotron emission was again detected, in this case by both ATCA and MOST (Staveley-Smith et al. 1992; Ball et al. 2001, respectively), marking the birth of the radio remnant. From the first radio detection, the radio emission has been regularly monitored every 1–2 months at 1.4, 2.4, 4.8 and 8.6 GHz using various array configurations of ATCA (Manchester et al. 2002; Staveley-Smith et al. 2007; Zanardo et al. 2010, and reference therein). At all these frequencies, the flux density has been steadily increasing over time and from $\sim$day 3000 after the explosion is growing exponentially, which is attributed to increasing efficient particle acceleration processes (Zanardo et al. 2010). On the other hand, the highest angular resolution observations ($\sim0''.1$) of the SNR obtained with the Australian Large Baseline Array (LBA) at 1.4 and 1.7 GHz revealed two extended lobes with an overall morphology in good agreement with that at lower angular resolutions. In addition, small-scale structures were found in the brightest regions in both lobes (Tingay et al. 2009; Ng et al. 2011).

Recently, Ng et al. (2013) reported on the study of the evolution of the radio morphology of the remnant of the SN 1987A covering the period January 1992–May 2013 (day 9568 after the explosion). The data were acquired with ATCA at 9 GHz with an angular resolution of $0''.4$. The remnant presents a double lobe ring, with an asymmetric surface brightness distribution with the eastern lobe brighter than its western counterpart (Fig. 15). From the analysis of this database, the authors point out that from day 7000 the asymmetry began to decline, such that the overall geometry is evolving towards a ring structure, suggesting that the remnant has entered in a new evolutionary stage where the forward shock has fully engulfed the entire inner ring and is now interacting with the densest part of the circumstellar medium.

Observations at higher frequencies (18, 36, 44 and 94 GHz) undertaken with ATCA (Manchester et al. 2005; Potter et al. 2009; Lakićević et al. 2012; Zanardo et al. 2013), followed by observations at 110, 215, and 345 GHz with the Atacama

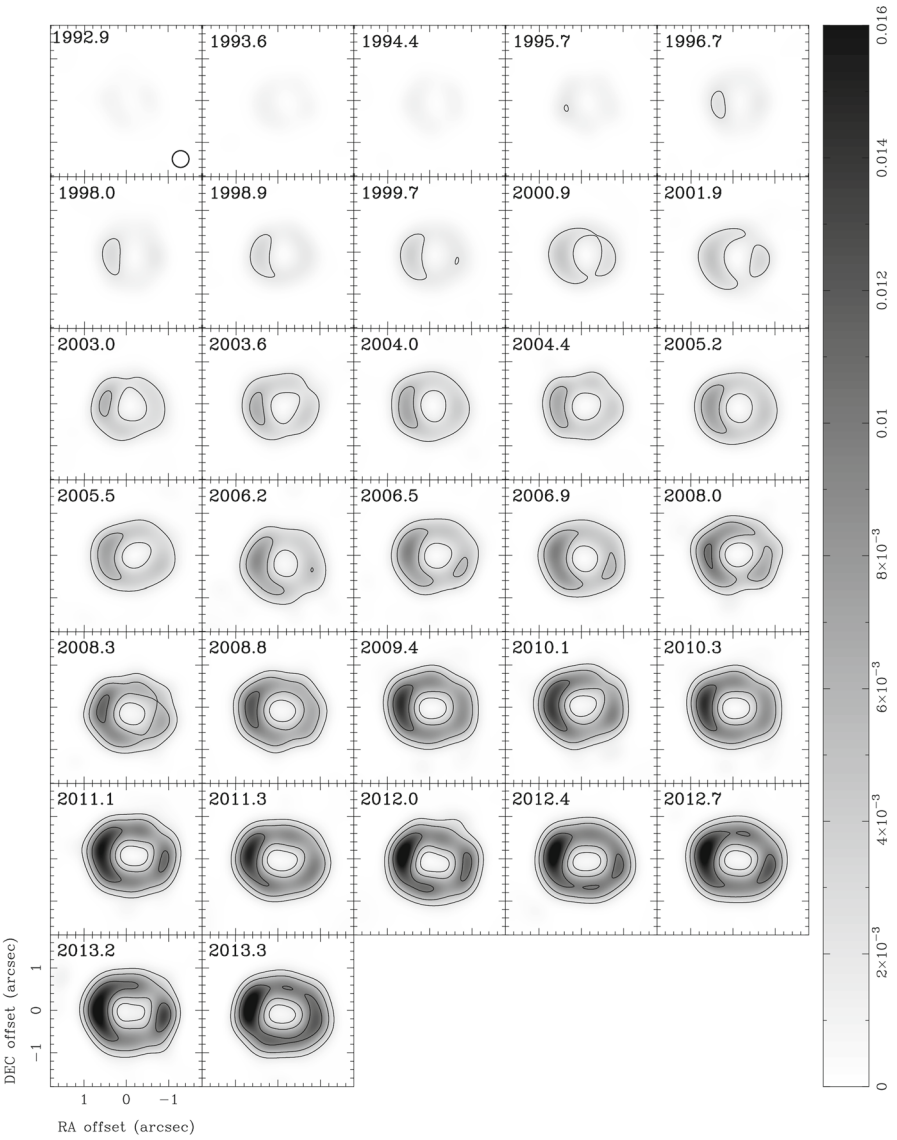

Fig. 15 9 GHz images of SN 1987A in the interval 1992–2013 obtained with an FWHM of $0''.4$ (figure provided by Ng et al. 2013)

Millimeter/Submillimeter Array (ALMA), show the same asymmetric double lobe morphology (Indebetouw et al. 2014; Zanardo et al. 2014). Also ALMA observations (Indebetouw et al. 2014) revealed the presence of one of the largest masses of cold dust (greater than 0.2 $M_{\odot}$) ever measured in an SNR. The dust emission is concentrated at the center of the remnant and has probably formed in the inner ejecta.

The evolution of the radio spectral index has been tracked over the years. At present, the mean spectral index estimated between the frequencies 18 and 44 GHz is $\alpha = 0.8$,

with values in the range 1.1–0.3 across the source. The brightest region on the eastern lobe is slightly steeper than the mean value, while flatter values, between 0.5 and 0.3, are found towards the central and the center-north regions of the SNR (Zanardo et al. 2013). The spectral index distribution of the synchrotron component was mapped in the frequencies range 44–672 GHz with data obtained with ATCA and ALMA instruments (Zanardo et al. 2014). From radio to far infrared, the authors estimate a mean spectral index for the synchrotron main component of 0.73, while a value ~ 0 was estimated around the central region and between 0.1 and 0.4 in the western half of the remnant. Zanardo et al. (2014) conclude that central region might be a PWN in the interior of the remnant, while the steepening of the spectral indices over the eastern lobe might be an indication of a local spectral break.

10 Conclusions and prospects of studies with the new generation radiotelescopes

Almost seven decades after the first detection of the radio emission coming from SNRs, great advances in the knowledge of their properties have been achieved. Detailed studies of the radio emission associated with SNRs have proven to be an excellent tool to recognize morphological characteristics, delineate the location of shock fronts, identify sites of interaction with dense clouds of the ISM, locate places of particle acceleration, and discover PWNe even in cases where the radio pulsar is not detected and the nebula is the only trace of its existence. They are also powerful probes of the magnetic field, providing information on the orientation and sites of higher compression. Furthermore, the possibility of resolving individual radio structures down to spatial scales of arcsec or even sub-arcsec, like in the expansion studies performed in Tycho's and SN1006 SNRs or the current studies of the Crab Nebula, is a powerful resource to investigate the dynamical evolution of SNRs.

Over the past years, key observations performed with single-dish telescopes and radio interferometers like ATCA, DRAO, VLA, VLBA, GMRT, etc. provided remarkable insights into radio SNRs. However, there still persist controversial issues and unsolved questions requiring further research from observational as well as theoretical approaches. In brief, particular issues deserving further observational studies are: the deficiencies of the spectral database, the generally poor quality of spatially resolved spectral indices over wide frequency ranges, the scarcity of well-determined distances, the incomplete knowledge of extended old SNRs, the missing (young and old) Galactic remnants, the consequences at all levels of the shock/cloud interactions, the alignment and strength of the magnetic field, and where and how particles are accelerated. From the theoretical point of view, the comprehension of SNRs would benefit from progress in the research of mechanisms of particle acceleration capable of explaining the variety of observed spectral indices, as well as from detailed modelling of the dynamical evolution of SNRs expanding in inhomogeneous environments.

Other motivation to increase the quality and accuracy of radio measurements is to match the ongoing revolution in high-energy (X-ray and γ-ray) studies. It is well known that recent surveys of the Milky Way with space and ground-based γ-ray detectors revealed hundreds of high-energy and tens of very-high-energy γ-ray emit-

ters representing several Galactic source populations, including numerous SNRs and PWNe whose emission mechanisms remain poorly constrained. The fundamental nature of many of the high-energy sources could greatly benefit from radio observations that are only recently becoming technically feasible, e.g. with the JVLA or ALMA.

Another area with pending studies is the investigation of faint SNRs, where the lack of precise information from radio data may affect the comprehension of high-energy phenomena and, at large, the question of the contribution of SNRs to the overall flux of Galactic cosmic rays. This is, for example, the case of the SNRs RX J1713.7-3946 and RX J0852.0-4622, two very interesting shell-type X-ray SNRs with bright γ-ray emission (at 1 TeV RX J0852.0-4622 is as bright as the Crab Nebula), but with poorly constrained radio parameters. These sources are radio weak, confused in parts with thermal emission and with significant Galactic background variation, characteristics that all together are detrimental to the accurate estimate of radio parameters. For cases like these, the new low-frequency synthesis arrays, like low-frequency array (LOFAR) in Europe, the Murchison widefield array (MWA) in Australia, and the Low-Band JVLA system in the USA, are important new tools. Their good sensitivity and angular resolution is key to imaging and differentiating the non-thermal radiation (bright at low radio frequencies) from optically thick and thin thermal emission from HII regions (which are intense at high-frequencies). Low radio frequency studies are also indispensable to improving the precision of the continuum spectra of all SNRs. Accurate low-frequency data anchor the spectrum, avoiding the uncertainties of extrapolation from higher frequency data which render them insensitive to curvature, an important piece of information to test the predictions of particle acceleration theories. In addition, sensitive high-resolution meter-wavelength studies of selected Galactic regions have already proven to be extremely useful to discover new SNRs. The detection of many new SNRs would alleviate the incompleteness of the current Galactic SNRs census with important implications for the SNe rate and energy input into the ISM. A deep meter-wavelength census of Galactic SNRs with the JVLA is currently under way, as are LOFAR studies of selected SNR complexes.

In the other extreme of radio frequencies, observations of radio-continuum emission of bright SNRs in the tens and hundreds of GHz regime using ATCA, ALMA, and JVLA, among other facilities, have come to fill in the gap between radio and IR, offering significantly improved constraints on SNRs spectral energy distributions.

The new aperture-synthesis telescopes, either in operation, commissioning, or in construction phase (EVLA, SKA and its precursors ASKAP in Australia, MeerKAT in South Africa, LWA in the USA, and FAST in China, plus the already mentioned MWA) will also bring important advances in understanding the properties of the magnetic field in SNRs. They will provide high angular resolution and will be able to produce wideband multichannel data amenable to rotation measure (RM) synthesis. Wide area polarization surveys will be very helpful to establish the presence of magnetic field, its direction, strength and spatial scale in a large sample of Galactic SNRs and in the Magellanic Clouds. In addition, very long baseline interferometers, like the European Network eEVN, are the appropriate instruments to resolve the structure and investigate the expansion of young SNRs located in nearby galaxies other than the Magellanic Clouds, following the pioneering studies conducted by Pedlar et al. (1999) in M 82

and Bartel et al. (1994) and Marcaide et al. (1995) in M 81, and the more recent from Bietenholz et al. (2010a) in NGC 4449, Bietenholz et al. (2010b) in NGC 891, etc.

Another chapter connected with the investigation of radio SNRs that deserves special attention is the study of the atomic and molecular emission from the surrounding ISM. Such studies have become more and more important to understand the properties of the SNRs across the whole electromagnetic spectrum. Large-scale HI surveys, like Southern Galactic Plane Survey (SGPS) in the southern hemisphere and VGPS (VLA Galactic Plane Survey) in the north, have been very helpful to explore in emission and absorption the characteristics of the ISM towards a large number of SNRs close to the Galactic plane. Also intermediate resolution CO surveys, like the GRS (Galactic Ring Survey of ^{13}CO in the northern sky) and the ^{12}CO NANTEN 4 m dish observations in the southern sky, have been important to localize possible sites of SNR/MC interaction. For sources at higher Galactic latitudes, the atomic and molecular studies require dedicated observations. The necessity, however, of more detailed studies of the surrounding ISM for a large number of SNRs is evident. An ample, good-quality atomic database will allow us to refine distance estimates and, particularly, HI data acquired with very high angular resolution and sensitivity can be the way to detect the HI shell predicted to form behind the expanding shock front when radiative cooling is sufficient to recombine a detectable amount of atomic material. On the other hand, molecular data at sub-arcmin angular resolution, as can be obtained with single-dish of intermediate size, like the 12 m antenna of the future Argentina–Brazil radiotelescope Long Latin American Millimetre Array (LLAMA), will be an adequate step forward following the NANTEN southern sky survey. The data will have the sensitivity and angular resolution suitable to cover large areas identifying compact molecular clumps that might have been overrun by SNRs.

In view of the present radio astronomy landscape, with new instruments already in use or coming into operation in the next future, plus upgrading of existing instruments with the latest technological developments, the panorama of future research of radio SNRs is very promising.

Acknowledgments We are very grateful to our colleagues Namir Kassim, David Green, and Gabriela Castelletti for the critical reading of this manuscript and useful comments. We thank CONICET (Argentina) for support through the Grant PIP 0736/11 and to ANPCyT (Argentina) through Grant PICT 0571/11. We have used images provided by C. Brogan, F. Giordano, L. Ksenofontov, C.-Y. Ng, S. Pineault, W. Reich, S. Reynolds, and E. Reynoso with permission of the authors, whom we thank.

References

Abdo AA, Ackermann M, Ajello M et al (2009) ApJ 706:L1
Abdo AA, Ackermann M, Ajello M et al (2010a) Science 327:1103
Abdo AA, Ackermann M, Ajello M et al (2010b) ApJ 722:1303
Abdo AA, Ajello M, Allafort A et al (2013) ApJS 208:17
Acciari VA, Aliu E, Arlen T et al (2009) ApJ 698:L133
Acero F, Ballet J, Decourchelle A et al (2009) A&A 505:157
Ackermann M, Ajello M, Allafort A et al (2013) Science 339:807
Aharonian F, Akhperjanian AG, Bazer-Bachi AR et al (2006) ApJ 636:777
Aharonian F, Akhperjanian AG, Bazer-Bachi AR et al (2008) A&A 481:401
Aharonian FA, Atoyan AM (1996) A&A 309:917

Aizu K, Tabara H (1967) Prog Theor Phys 37:296
Alfvén H, Herlofson N (1950) Phys Rev 78:616
Amy SW, Ball L (1993) ApJ 411:761
Anderl S, Gusdorf A, Güsten R (2014) A&A 569:A81
Araya M (2013) MNRAS 434:2202
Arbutina B, Urošević D, Stanković M, Tešić L (2004) MNRAS 350:346
Arendt RG, Dwek E, Blair WP et al (2010) ApJ 725:585
Auchettl K, Slane P, Castro D (2014) ApJ 783:32
Baade W, Minkowski R (1954) ApJ 119:206
Badenes C, Maoz D, Draine BT (2010) MNRAS 407:1301
Ball L, Crawford DF, Hunstead RW, Klamer I, McIntyre VJ (2001) ApJ 549:599
Ballet J (2006) Adv Space Res 37:1902
Bartel N, Bietenholz M-F, Rupen M-P, Conway J-E, Beasley A-J, Sramek R-A, Romney J-D, Titus M-A, Graham D-A, Altunin V-I, Jones DL, Rius A, Venturi T, Umana G, Francis R-L, McCall M-L, Richer MG, Stevenson C-C, Weiler K-W, van Dyk S-D, Panagia N, Cannon W-H, Popelar J, Davis R-J (1994) The shape, expansion rate and distance of supernova 1993J from VLBI measurements. Nature 368:610–613. doi:10.1038/368610a0
Beck R (2012) in EAS Publications Series, Vol. 56, EAS Publications Series, ed. M. A. de Avillez, 51–59
Bell AR (1978a) MNRAS 182:147
Bell AR (1978b) MNRAS 182:443
Bell AR, Schure KM, Reville B (2011) MNRAS 418:1208
Beresnyak A, Jones TW, Lazarian A (2009) ApJ 707:1541
Berezhko EG, Ksenofontov LT, Völk HJ (2012) ApJ 759:12
Berezhko EG, Völk HJ (2000) Astropart Phys 14:201
Bhattacharjee P, Chaudhury S, Kundu S (2014) ApJ 785:63
Bietenholz MF, Bartel N, Milisavljevic D et al (2010a) MNRAS 409:1594
Bietenholz MF, Bartel N, Rupen MP (2010b) ApJ 712:1057
Bietenholz M-F, Yuan Y, Buehler R, Lobanov A-P, Blandford R (2015) The variability of the Crab Nebula in radio: no radio counterpart to gamma-ray flares. MNRAS 446:205–216. doi:10.1093/mnras/stu2025
Blandford R, Eichler D (1987) Phys Rep 154:1
Blandford RD, Ostriker JP (1978) ApJ 221:L29
Bolatto AD, Wolfire M, Leroy AK (2013) ARA&A 51:207
Borkowski KJ, Reynolds SP, Green DA et al (2010) ApJ 724:L161
Borkowski KJ, Reynolds SP, Hwang U et al (2013) ApJ 771:L9
Bozzetto LM, Filipović MD, Crawford EJ et al (2013) MNRAS 432:2177
Brentjens MA, de Bruyn AG (2005) A&A 441:1217
Brogan CL, Frail DA, Goss WM, Troland TH (2000) ApJ 537:875
Brogan CL, Lazio TJ, Kassim NE, Dyer KK (2005) AJ 130:148
Brogan CL, Gelfand JD, Gaensler BM, Kassim NE, Lazio TJW (2006) ApJ 639:L25
Brun F, de Naurois M, Hofmann W, et al. (2011), in SF2A-2011: Proceedings of the Annual meeting of the French Society of Astronomy and Astrophysics, ed. Alecian, G, Belkacem K, Samadi R, Valls-Gabaud D, 545–548
Burbidge GR (1959) ApJ 129:849
Burn BJ (1966) MNRAS 133:67
Burrows CJ, Krist J, Hester JJ et al (1995) ApJ 452:680
Butt Y (2009) Nature 460:701
Case GL, Bhattacharya D (1998) ApJ 504:761
Cassam-Chenaï G, Decourchelle A, Ballet J et al (2004) A&A 427:199
Castelletti G, Dubner G, Golap K, Goss WM (2006) A&A 459:535
Castelletti G, Dubner G, Brogan C, Kassim NE (2007) A&A 471:537
Castelletti G, Dubner G, Clarke T, Kassim NE (2011a) A&A 534:A21
Castelletti G, Giacani E, Dubner G et al (2011b) A&A 536:A98
Castro D, Slane P, Carlton A, Figueroa-Feliciano E (2013) ApJ 774:36
Castro D, Slane P (2010) ApJ 717:372
Chen Y, Jiang B (2013) Scientia Sinica Physica Mechanica Astronomica 43:1
Chevalier RA (1974) ApJ 188:501
Chevalier RA (1982a) ApJ 259:L85

Chevalier RA (1982b) ApJ 258:790
Chevalier RA (1998) ApJ 499:810
Clark DH, Caswell JL (1976) MNRAS 174:267
Claussen MJ, Frail DA, Goss WM, Gaume RA (1997) ApJ 489:143
Combi JA, Albacete-Colombo JF, Martí J (2008) A&A 488:L25
Combi JA, Albacete Colombo JF, Sánchez-Ayaso E et al (2010) A&A 523:A76
Cornett RH, Chin G, Knapp GR (1977) A&A 54:889
Cox DP (2005) ARA&A 43:337
Crotts APS, Heathcote SR (2000) ApJ 528:426
DeLaney T, Koralesky B, Rudnick L, Dickel JR (2002) ApJ 580:914
DeLaney T, Kassim NE, Rudnick L, Perley RA (2014) ApJ 785:7
Desai KM, Chu Y-H, Gruendl RA et al (2010) AJ 140:584
Dickel JR, Dickel HR, Crutcher RM (1976) PASP 88:840
Dickel JR, Milne DK, Junkes N, Klein U (1993) A&A 275:265
Dickel JR, Milne DK (1995) AJ 109:200
Dickel JR, Milne DK (1998) AJ 115:1057
Downes D (1971) AJ 76:305
Drury LO, Downes TP (2012) MNRAS 427:2308
Dubner GM, Giacani EB, Goss WM, Winkler PF (1994) AJ 108:207
Dubner GM, Holdaway M, Goss WM, Mirabel IF (1998) AJ 116:1842
Dubner GM, Velázquez PF, Goss WM, Holdaway MA (2000) AJ 120:1933
Dubner GM, Gaensler BM, Giacani EB, Goss WM, Green AJ (2002) AJ 123:337
Dubner G, Giacani E, Reynoso E, Parón S (2004) A&A 426:201
Dubner G, Loiseau N, Rodríguez-Pascual P et al (2013) A&A 555:A9
Dubner GM, Arnal EM (1988) A&A 75:363
Dumas G, Vaupré S, Ceccarelli C et al (2014) ApJ 786:L24
Dwarkadas VV (2005) ApJ 630:892
Ellison DC, Bykov AM (2011) ApJ 731:87
Ellison DC, Reynolds SP (1991) ApJ 382:242
Feinstein F, Fiasson A, Gallant Y et al (2009) In: Bastieri D, Rando R (eds) American Institute of Physics Conference Series, vol 1112, pp 54–62
Fermi E (1949) Phys Rev 75:1169
Ferrand G, Safi-Harb S (2012) Adv Space Res 49:1313
Frail DA, Giacani EB, Goss WM, Dubner G (1996a) ApJ 464:L165
Frail DA, Goss WM, Reynoso EM et al (1996b) AJ 111:1651
Frail DA, Mitchell GF (1998) ApJ 508:690
Fukui Y, Sano H, Sato J et al (2012) ApJ 746:82
Fürst E, Reich W (2004) In: Uyaniker B, Reich W, Wielebinski R (eds) The magnetized interstellar medium, pp 141–146
Gabici S, Aharonian FA, Casanova S (2009) MNRAS 396:1629
Gaensler BM (1998) ApJ 493:781
Gaensler BM, Brazier KTS, Manchester RN, Johnston S, Green AJ (1999) MNRAS 305:724
Gaensler BM, Arons J, Kaspi VM et al (2002) ApJ 569:878
Gaensler BM, Slane PO (2006) ARA&A 44:17
Gaensler BM, Wallace BJ (2003) ApJ 594:326
Gardner FF, Whiteoak JB (1966) ARA&A 4:245
Gelfand JD, Castro D, Slane PO et al (2013) ApJ 777:148
Ghavamian P, Long KS, Blair WP et al (2012) ApJ 750:39
Giacani EB, Dubner GM, Kassim NE et al (1997) AJ 113:1379
Giacani EB, Dubner GM, Green AJ, Goss WM, Gaensler BM (2000) AJ 119:281
Giacani E, Smith MJS, Dubner G et al (2009) A&A 507:841
Giacani E, Smith MJS, Dubner G, Loiseau N (2011) A&A 531:A138
Ginzburg VL, Syrovatskii SI (1965) ARA&A 3:297
Giordano F, Naumann-Godo M, Ballet J et al (2012) ApJ 744:L2
Giuliani A, Cardillo M, Tavani M et al (2011) ApJ 742:L30
Goss WM, Robinson BJ (1968) Astrophys Lett 2:81
Green DA (1984) MNRAS 209:449

Green DA (1991) PASP 103:209
Green AJ, Frail DA, Goss WM, Otrupcek R (1997) AJ 114:2058
Green DA, Reynolds SP, Borkowski KJ et al (2008) MNRAS 387:L54
Green DA (2014) Bull Astron Soc India 42:47
Grondin M-H, Sasaki M, Haberl F et al (2012) A&A 539:A15
Han JL, Gao XY, Sun XH et al (2014) In: Ray A, McCray RA (eds) IAU symposium, vol 296, pp 202–209
Hanabata Y, Katagiri H, Hewitt JW et al (2014) ApJ 786:145
Hansen BMS, Phinney ES (1997) MNRAS 291:569
Harvey-Smith L, Gaensler BM, Kothes R et al (2010) ApJ 712:1157
Harwit M (1988) Astrophysical concepts. Springer, Berlin
Hayakawa T, Torii K, Enokiya R, Amano T, Fukui Y (2012) PASJ 64:8
Heald G, Braun R, Edmonds R (2009) A&A 503:409
Heiles C (1984) ApJS 55:585
Hewitt JW, Yusef-Zadeh F, Wardle M (2008) ApJ 683:189
Huang Y-L, Thaddeus P (1986) ApJ 309:804
Hughes JP, Hayashi I, Helfand D et al (1995) ApJ 444:L81
Hwang U, Laming JM, Badenes C et al (2004) ApJ 615:L117
Hwang U, Flanagan KA, Petre R (2005) ApJ 635:355
Ilovaisky SA, Lequeux J (1972) A&A 18:169
Indebetouw R, Matsuura M, Dwek E et al (2014) ApJ 782:L2
Jansky KG (1933) Pop Astron 41:548
Jiang B, Chen Y, Wang J et al (2010) ApJ 712:1147
Jones TW, Rudnick L, Jun B-I et al (1998) PASP 110:125
Jones TW (2011) J Astrophys Astron 32:427
Jun B-I, Norman ML, Stone JM (1995) ApJ 453:332
Jun B-I, Norman ML (1996) ApJ 465:800
Kassim NE (1989) ApJS 71:799
Kassim NE, Hertz P, van Dyk SD, Weiler KW (1994) ApJ 427:L95
Kassim NE, Perley RA, Dwarakanath KS, Erickson WC (1995) ApJ 455:L59
Katz-Stone DM, Kassim NE, Lazio TJW, O'Donnell R (2000) ApJ 529:453
Katz-Stone DM, Rudnick L (1997) ApJ 479:258
Kavanagh PJ, Sasaki M, Points SD et al (2013) A&A 549:A99
Kiepenheuer KO (1950) Phys Rev 79:738
Kilpatrick CD, Bieging JH, Rieke GH (2014) ApJ 796:144
Koo B-C, Rho J, Reach WT, Jung J, Mangum JG (2001) ApJ 552:175
Koo B-C, McKee CF, Lee J-J et al (2008) ApJ 673:L147
Koo B-C, Kang J-H (2004) MNRAS 349:983
Koo B-C, Moon D-S (1997) ApJ 485:263
Koralesky B, Frail DA, Goss WM, Claussen MJ, Green AJ (1998) AJ 116:1323
Kothes R (2003) A&A 408:187
Krassilchtchikov A, Bykov A, Kargaltsev O et al (2014) In: COSPAR meeting, 40th COSPAR scientific assembly, vol 40, Held 2–10 August 2014, Moscow, Russia, Abstract E1.16-10-14., 1643
Lacey CK, Lazio TJW, Kassim NE et al (2001) ApJ 559:954
Lakićević M, Zanardo G, van Loon JT et al (2012) A&A 541:L2
Landecker TL, Pineault S, Routledge D, Vaneldik JF (1982) ApJ 261:L41
Landecker TL, Pineault S, Routledge D, Vaneldik JF (1989) MNRAS 237:277
Landecker TL, Routledge D, Reynolds SP et al (1999) ApJ 527:866
Landecker TL (2012) Space Sci Rev 166:263
Lazendic JS, Wardle M, Burton MG et al (2004) MNRAS 354:393
Leahy DA, Roger RS (1998) ApJ 505:784
Leahy DA, Tian WW (2008) A&A 480:L25
Lee J-J, Koo B-C, Yun MS et al (2008) AJ 135:796
Lequeux J (2005) The interstellar medium. Springer, Berlin
Li H, Chen Y (2012) MNRAS 421:935
Lopez LA, Ramirez-Ruiz E, Badenes C et al (2009) ApJ 706:L106
Lopez LA, Ramirez-Ruiz E, Huppenkothen D, Badenes C, Pooley DA (2011) ApJ 732:114
Maggi P, Haberl F, Bozzetto LM et al (2012) A&A 546:A109

Maggi P, Haberl F, Kavanagh PJ et al (2014) A&A 561:A76
Malkov MA, O'C Drury L (2001) Rep Prog Phys 64:429
Manchester RN (1987) A&A 171:205
Manchester RN, Mar DP, Lyne AG, Kaspi VM, Johnston S (1993a) ApJ 403:L29
Manchester RN, Staveley-Smith L, Kesteven MJ (1993b) ApJ 411:756
Manchester RN, Gaensler BM, Wheaton VC et al (2002) PASA 19:207
Manchester RN, Gaensler BM, Staveley-Smith L, Kesteven MJ, Tzioumis AK (2005) ApJ 628:L131
Maoz D, Mannucci F, Nelemans G (2014) ARA&A 52:107
Marcaide JM, Alberdi A, Ros E et al (1995) Nature 373:44
Mathewson DS, Ford VL, Dopita MA et al (1983) ApJS 51:345
Mathewson DS, Healey JR (1963) Nature 199:681
Mayer CH, McCullough TP, Sloanaker RM (1957) ApJ 126:468
Mayer CH, Hollinger JP (1968) ApJ 151:53
McClure-Griffiths NM, Dickey JM, Gaensler BM, Green AJ (2002) ApJ 578:176
McKee CF, Ostriker JP (1977) ApJ 218:148
Melioli C, de Gouveia Dal Pino EM, de La Reza R, Raga A (2006) MNRAS 373:811
Miceli M, Acero F, Dubner G et al (2014) ApJ 782:L33
Milne DK (1968) Aust J Phys 21:201
Milne DK (1970) Aust J Phys 23:425
Milne DK (1980) A&A 81:293
Milne DK (1987) Aust J Phys 40:771
Milne DK, Dickel JR (1975) Aust J Phys 28:209
Moffet AT (1975) In: Sandage A, Sandage M, Kristian J (eds) Strong nonthermal radio emission from galaxies: galaxies and the universe. University of Chicago Press, Chicago, 211
Moriguchi Y, Yamaguchi N, Onishi T, Mizuno A, Fukui Y (2001) PASJ 53:1025
Moriguchi Y, Tamura K, Tawara Y et al (2005) ApJ 631:947
Ng C-Y, Potter TM, Staveley-Smith L et al (2011) ApJ 728:L15
Ng C-Y, Zanardo G, Potter TM et al (2013) ApJ 777:131
Odenwald SF, Shivanandan K (1985) ApJ 292:460
Ojeda-May P, Kurtz SE, Rodríguez LF, Arthur SJ, Velázquez P (2002) Rev Mexicana Astron Astrofis 38:111
Opik EJ (1953) Ir Astron J 2:219
Ostrowski M (1999) A&A 345:256
Pacholczyk AG (1970) Radio astrophysics. Nonthermal processes in galactic and extragalactic sources. Freeman, San Francisco
Parizot E, Marcowith A, Ballet J, Gallant YA (2006) A&A 453:387
Park S, Roming PWA, Hughes JP et al (2002) ApJ 564:L39
Park S, Hughes JP, Slane PO et al (2004) ApJ 602:L33
Park S, Hughes JP, Slane PO et al (2007) ApJ 670:L121
Park G, Koo B-C, Gibson SJ et al (2013) ApJ 777:14
Paron SA, Reynoso EM, Purcell C, Dubner GM, Green A (2006) PASA 23:69
Paron S, Dubner G, Reynoso E, Rubio M (2008) A&A 480:439
Paron S, Ortega ME, Rubio M, Dubner G (2009) A&A 498:445
Paron S, Ortega ME, Petriella A et al (2012) A&A 547:A60
Patnaude DJ, Fesen RA (2007) AJ 133:147
Pavlovic MZ, Dobardzic A, Vukotic B, Urosevic D (2014) Serbian Astron J 189:25
Pedlar A, Muxlow TWB, Garrett MA et al (1999) MNRAS 307:761
Peters CL, Lopez LA, Ramirez-Ruiz E, Stassun KG, Figueroa-Feliciano E (2013) ApJ 771:L38
Petre R, Kriss GA, Winkler PF, Canizares CR (1982) ApJ 258:22
Petruk O, Dubner G, Castelletti G et al (2009) MNRAS 393:1034
Phillips JP, Ramos-Larios G, Perez-Grana JA (2009) MNRAS 397:1215
Pineault S, Landecker TL, Routledge D (1987) ApJ 315:580
Potter TM, Staveley-Smith L, Ng C-Y et al (2009) ApJ 705:261
Poveda A, Woltjer L (1968) AJ 73:65
Reach WT, Rho J, Jarrett TH (2005) ApJ 618:297
Reach WT, Rho J (1999) ApJ 511:836
Reber G (1944) ApJ 100:279
Reich W (2006) ArXiv Astrophysics e-prints

Reichardt I, de Oña-Wilhelmi E, Rico J, Yang R (2012) A&A 546:A21
Reynolds SP (2008) ARA&A 46:89
Reynolds SP, Borkowski KJ, Green DA et al (2008) ApJ 680:L41
Reynolds SP, Borkowski KJ, Green DA et al (2009) ApJ 695:L149
Reynolds SP (2011) Ap&SS 336:257
Reynolds SP, Gaensler BM, Bocchino F (2012) Space Sci Rev 166:231
Reynolds SP, Ellison DC (1992) ApJ 399:L75
Reynolds SP, Gilmore DM (1986) AJ 92:1138
Reynolds SP, Gilmore DM (1993) AJ 106:272
Reynoso EM, Dubner GM, Goss WM, Arnal EM (1995) AJ 110:318
Reynoso EM, Velázquez PF, Dubner GM, Goss WM (1999) AJ 117:1827
Reynoso EM, Hughes JP, Moffett DA (2013) AJ 145:104
Rho J, Petre R (1998) ApJ 503:L167
Rohlfs K (1990) Tools of radio astronomy. Springer, Berlin
Rohlfs K, Wilson TL (1996) Tools of radio astronomy. Springer, Berlin
Routledge D, Dewdney PE, Landecker TL, Vaneldik JF (1991) A&A 247:529
Ryle M, Smith FG (1948) Nature 162:462
Sashida T, Oka T, Tanaka K et al (2013) ApJ 774:10
Sato F (1974) PASJ 26:459
Sazonov VN (1973) Soviet Ast 16:774
Schure KM, Bell AR, O'C Drury L, Bykov AM (2012) Space Sci Rev 173:491
Sedov LI (1959) Similarity and dimensional methods in mechanics. CRC Press, Boca Raton
Seta M, Hasegawa T, Dame TM et al (1998) ApJ 505:286
Seta M, Hasegawa T, Sakamoto S et al (2004) AJ 127:1098
Shklovsky IS (1960a) Soviet Ast 4:243
Shklovsky IS (1960b) Soviet Ast 4:355
Shklovsky JS (1978) Stars, their birth, life and death. Izdatel'stvo Nauka, Moscow
Slane P, Bykov A, Ellison DC, Dubner G, Castro D (2015) Space Sci Rev 188:187
Smartt SJ (2009) ARA&A 47:63
Staveley-Smith L, Manchester RN, Kesteven MJ et al (1992) Nature 355:147
Staveley-Smith L, Gaensler BM, Manchester RN et al (2007) In: Immler S, Weiler K, McCray R (eds) American Institute of Physics Conference Series, Supernova 1987A: 20 years after: supernovae and gamma-ray bursters, vol 937, pp 96–101
Storey MC, Manchester RN (1987) Nature 329:421
Su Y, Fang M, Yang J, Zhou P, Chen Y (2014) ApJ 788:122
Suad LA, Caiafa CF, Arnal EM, Cichowolski S (2014) A&A 564:A116
Taylor G (1950) R Soc Lond Proc Ser A 201:159
Tian WW, Leahy DA (2008) MNRAS 391:L54
Tielens AGGM (2005) The physics and chemistry of the interstellar medium. Cambridge University Press, Cambridge
Tingay S, Phillips C, Amy S et al (2009) In: 8th international e-VLBI workshop, 100
Toledo-Roy JC, Velázquez PF, Esquivel A, Giacani E (2014) MNRAS 437:898
Trimble V (1973) PASP 85:579
Truelove JK, McKee CF (1999) ApJS 120:299
Turtle AJ, Campbell-Wilson D, Bunton JD et al (1987) Nature 327:38
Uchida KI, Morris M, Bally J, Pound M, Yusef-Zadeh F (1992) ApJ 398:128
Uchiyama Y, Aharonian FA, Tanaka T, Takahashi T, Maeda Y (2007) Nature 449:576
Urošević D (2014) Ap&SS 354:541
van der Laan H (1962) MNRAS 124:125
Vanhala HAT, Cameron AGW (1998) ApJ 508:291
Velázquez PF, Dubner GM, Goss WM, Green AJ (2002) AJ 124:2145
Verschuur GL, Kellermann KI (1988) Galactic and extra-galactic radio astronomy. Springer, Berlin
Vink J (2012) A&Ar 20:49
Völk HJ, Berezhko EG, Ksenofontov LT (2005) A&A 433:229
Weiler KW, Sramek RA (1988) ARA&A 26:295
Whiteoak JB, Gardner FF (1968) ApJ 154:807
Wielebinski R (2012) J Astron Hist Herit 15:76

Williams JP, Blitz L, McKee CF (2000) Protostars and planets IV, 97
Wilson TL (1970) Astrophys Lett 7:95
Winkler PF, Long KS (2006) AJ 132:360
Woltjer L (1972) ARA&A 10:129
Wood CA, Mufson SL, Dickel JR (2008) AJ 135:2358
Wootten HA (1977) ApJ 216:440
Wootten A (1978) Moon Planets 19:163
Wu JHK, Wu EMH, Hui CY et al (2011) ApJ 740:L12
Xu J-L, Wang J-J, Miller M (2011) ApJ 727:81
Yamaguchi H, Badenes C, Petre R et al (2014) ApJ 785:L27
Yusef-Zadeh F, Roberts DA, Goss WM, Frail DA, Green AJ (1996) ApJ 466:L25
Zanardo G, Staveley-Smith L, Ball L et al (2010) ApJ 710:1515
Zanardo G, Staveley-Smith L, Ng C-Y et al (2013) ApJ 767:98
Zanardo G, Staveley-Smith L, Indebetouw R et al (2014) ApJ 796:82
Zhang Z, Gao Y, Wang J (2010) Sci China Phys Mech Astron 53:1357
Zhu H, Tian WW, Zuo P (2014) ApJ 793:95